Development of Fault Detection and Diagnosis Techniques with Applications to Fixed-wing and Rotary-wing UAVs

Ling Ma

A Thesis

in

The Department

of

Mechanical and Industrial Engineering

Presented in Partial Fulfillment of the Requirements

for the Degree of Master of Applied Science (Mechanical Engineering) at

Concordia University

Montreal, Quebec, Canada

January 2011

CONCORDIA UNIVERSITY

School of Graduate Studies

This is to certify that the thesis prepared

By: Ling Ma

Entitled:

and submitted in partial fulfillment of the requirements for the degree of

Master of Applied Science (Mechanical Engineering)

complies with the regulations of the University and meets the accepted standards with respect to originality and quality.

Signed by the final examining committee:

_____ Chair

_____Wei Ping Zhu___ Examiner

_____Henry Hong____ Examiner

_____ You Min Zhang__Supervisor

Approved by

_____

Chair of Department of Graduate Program Director

_____20__ _____

Dean of Faculty

ABSTRACT

Development of Fault Detection and Diagnosis Techniques with Applications to Fixed-wing and Rotary-wing UAVs

Ling Ma

Fault Detection and Diagnosis (FDD), as the central part of a Fault Tolerant Control System (FTCS), detects and diagnoses the source and the magnitude of a fault when a fault/failure occurs either in an actuator, sensor or in the system itself. This thesis work develops an applicable procedure for a FDD scheme to both fixed-wing and rotary-wing UAVs (Unmanned Aerial Vehicles) in the discrete-time stochastic domain based on the Kalman filter techniques. In particular, the proposed techniques are developed in highly nonlinear and 6 degree-of-freedom equations of Matlab/Simulink simulation environment for a quad-rotor helicopter UAV, a Boeing 747, and a NASA Generic Transport Model (GTM) fixed-wing UAV. A key development in this thesis is that an Adaptive Two-Stage Extended Kalman Filter (ATSEKF) algorithm and a Dual Unscented Kalman Filter (DUKF) algorithm are applied for simultaneous states and fault parameters estimation of these UAVs. The statistical decision-making techniques for fault detection and diagnosis are also discussed in the presence of partial faults in the UAVs. The measured system outputs and control signals are used as inputs of the ATSEKF and DUKF, and the estimated states and parameters are used for comparison and analysis in the fault detection and diagnosis. The simulation results show that the effectiveness and performance of ATSEKF and DUKF for the purpose of fault detection and diagnosis of both fixed- and rotary-wing UAVs are satisfactory.

Acknowledgements

I am grateful to my supervisor, Professor Youmin Zhang, for his support and guidance throughout my work. This work would have never been done without his advice and comments. I also highly appreciate him for being infinitely genuine, kind and considerate towards me.

I would like to thank all my friends, especially Xiaobing Zhang, Qingli Zhou and Yinhua Sun who gave me lots of support during the research.

Last, but not least, I would like to thank my mother, my husband and my daughter. Without their help and encouragement, I could not finish this study. Especially, I thank Yuzhuo Wang for being so generous in taking care of my daughter so that I could concentrate on my research and study. You mean everything to me.

TABLE OF CONTENT

List of Figures

List of Tables

List of Abbreviations

AFTCS	Active Fault Tolerant Control System
DUKF	Dual Unscented Kalman Filter
EAS	Equivalent Air Speed
EKF	Extended Kalman Filter
FDD	Fault Detection and Diagnosis
FTC	Fault Tolerant Control
GTM	Generic Transport Model
LPV	Linear Parameter Varying
PE	Parameter Estimation
PFTCS	Passive Fault Tolerant Control System
PID	Proportional-Integral-Derivative
TSKF	Two-Stage Kalman Filter
ATSEKF	Adaptive Two-Stage Extended Kalman Filter
UAV	Unmanned Aerial Vehicle
UKF	Unscented Kalman Filter
UT	Unscented Transform

QTA	Qualitative Trend Analysis
SPC	Statistical Process Control
PCA	Principal Component Analysis
PLS	Partial Least Squares
NN	Neural Networks

Nomenclature

m	Mass of quad-rotor UAV
ϕ	Roll angle fixed with Earth frame
θ	Pitch angle fixed with Earth frame
ψ	Yaw angle fixed with Earth frame
β	Sideslip angle fixed with Earth frame
α	Angle of attack
p	Roll angular rate
q	Pitch angular rate
r	Yaw angular rate
x	Position along x-axis
y	Position along y-axis
z	Position along z-axis
u	Velocity along x-axis with body frame
v	Velocity along y-axis with body frame
w	Velocity along z-axis with body frame
V	Total velocity

I_x	The inertia around *x*-axis
I_y	The inertia around *y*-axis
I_z	The inertia around *z*-axis
$I_{xx}, I_{xz}, I_{yy} \ldots$	Mass & products of inertia
L	Lift force
C_d	Drag coefficient
C_L	Lift coefficient
C_l	Rolling moment coefficient
C_m	Pitching moment coefficient
C_n	Yawing moment coefficient
C_Y	Side force coefficient
D	Drag force
δ_e	Elevation deflection
δ_t	Throttle deflection
δ_s	Stabilization deflection
T	Engine thrust

ω	Rotation speed of aircraft
$F_1, F_2, F_{3,} F_4$	Thrusts generated by corresponding rotor blades
$\bar{c}$	Wing chord
$\bar{q}$	Dynamic pressure, $\frac{1}{2}\rho V_{TAS}{}^2$

1 Introduction

The conventional feedback control system design is difficult for achieving desired performance in the event of fault occurrence, even for maintaining system stability after a fault occurrence. Due to the growing demand on dynamical systems to run autonomously in the presence of faults, industries in various areas spend time and money to develop intelligent or adaptive systems that are able to detect the presence of faults and isolate the faulty components in systems, especially in the aircraft industry. Since 1970s, the Fault Detections and Diagnosis (FDD) technique has been widely studied and used to isolate the faults and to accomplish satisfactory tasks under degraded situations when faults happen. FDD is utilized as the central part of an Active Fault Tolerant Control System (AFTCS) which is different from the conventional control system due to its ability to provide an acceptable level of performance and to maintain system stability even in the presence of faults, which could occur in the actuators, sensors or other system components. Therefore, the motivation of FDD is to provide the information about faults (time, type and magnitude) once a fault occurs. Based on the provided information by FDD, AFTCS can achieve successful system control reconfiguration [1, 2]. Development and implementation of FDD techniques for an AFTCS is presented in this thesis.

1.1 Motivation

For the aviation industry, the safety of aircraft passengers has always been an important issue. In history, a number of aircraft disasters were due to the damaged

aircrafts making the aircraft out of control during the flight. The followings are two examples that motivate people to examine and investigate practical FDD techniques in the aircraft industry.

Figure 1-1 Americal Airlines Flight 191, 1979 [13]

As shown in Figure 1-1, on May 25, 1979, American Airlines Flight 191, operated by a McDonnell Douglas DC-10-10, crashed on takeoff from Chicago. Investigators found that the #1 engine and pylon separated from the wing during rotation and a leak in the hydraulic lines allowed the left-side slats to retract, while the right-side slats remained extended. This led to a stall on the left wing which resulted in the roll-over. The airplane had 258 passengers and 13 crews on board. All of them died along with two on the ground. This is the deadliest crash in United States history [13].

Figure 1-2 An L-1011, Delta Airlines Flight 1080, 1977 [64]

The next example [64] shows that the damaged aircrafts still can be controlled and safely landed. On April 1977, an L-1011, Delta Airlines Flight 1080 took off from San Diego with an undetected failure where the left stabilizer jammed in the full trailing-edge-up position, see Figure 1-2. The nose-up and rolling moment were too large to be controlled. Fortunately, the experienced captain successfully landed the airplane safely by using throttles to supplement the remaining flight controls, using differential and collective engine thrust.

Occurrence of these types of accidents leads to increasing interests in the emerging field of FTCS and FDD [43]. It is suggested that a successful FDD system can help crew members to detect and point out faults and failures with detailed information and solutions promptly in order to handle the problems of the aircraft at the initial stage. When the crews encounter something wrong with the aircraft, if there were a FDD

system to point out the faults and failures in detail and give the solution timely, they may be able to handle it. In the presence of a FDD system, the degree of danger of the faults or failures could be decreased, the probability of the safety of aircrafts could be increased, and therefore the lives of passengers could be protected. The $500 million NASA Aviation Safety Program was initiated in 1997 [61], and the objective is to develop advanced and affordable technologies to reduce the fatal aircraft accident rate. FDD is therefore critical and necessary for the safe operation of aerial vehicles in the aviation industry.

1.2 Literature Review

In this part, a literature review of the existing FDD techniques is presented. In order to understand the FDD better, FTCS is introduced first briefly. Zhang and Jiang [3] define the FTCS as "control systems that possess the ability to accommodate system component failures automatically. They are capable of maintaining overall system stability and acceptable performance in the event of such failures". FTCS were also known as self-repairing, reconfigurable or self-designing control systems. Existing FTCS can be divided into two groups:

1) The Passive FTCS (PFTCS) that does not include controller reconfiguration;
2) The Active FTCS (AFTCS) that integrates controller reconfiguration based on the outputs of a FDD module.

The difference between PFTCS and AFTCS is that the controllers in PFTCS are designed to be robust against a class of presumed faults, while the controllers in AFTCS

can be reconstructed on-line in case of faults occurring in the system. Obviously, AFTCS is dependent on a FDD process to monitor system performance and to detect and identify faults in the systems [4].

As shown in Figure 1-3, a typical AFTCS consists of four sub-components [5]:

a) A sufficiently robust controller which is reconfigurable;
b) A FDD scheme with high sensitivity to faults and low sensitivity to disturbances;
c) A reconfiguration mechanism to reconfigure the system as much as possible;
d) A command/reference governor.

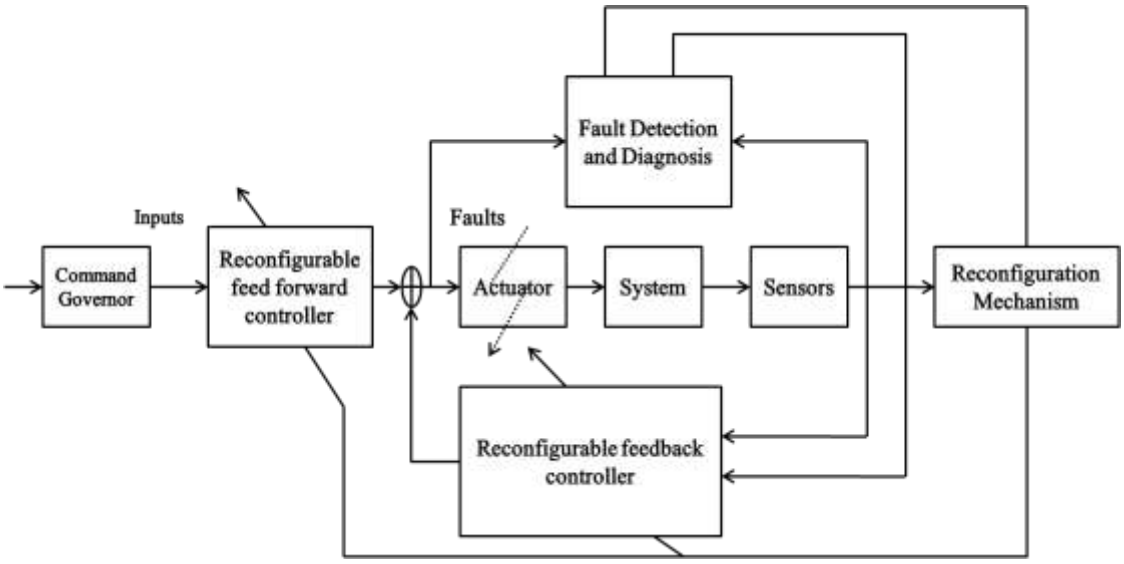

Figure 1-3 General structure of AFTCS [3]

A FDD scheme with high sensitivity to faults and low sensitivity to model uncertainties, operating condition variations, and external disturbances [3] is one of key issues of AFTCS. Hence, the objective of a good FDD scheme is to provide fault

information on the system to the reconfiguration mechanism as precisely and timely as possible in an AFTCS. This thesis work will focus on the development of new approaches to FDD schemes for nonlinear systems. As mentioned above, the goal of a FDD scheme is to make the planned operation succeed by identifying anomalies of the system behavior. Hence, a FDD scheme in AFTCS has three main objectives:

1) **Fault detection**, which indicates that something in the system is wrong, and provides information on the occurrence of a fault and the time of the fault occurrence. A fault can be any type of malfunction in sensors, actuators and components of the system that degrades the system performance and even leads the system to crush. In the flight control system, failures in the actuator or sensor may have depressed consequences that need to be detected as soon and precisely as possible;
2) **Fault isolation**, which is to determine the location and type of the fault (which component has failed);
3) **Fault identification**, which is to obtain the magnitude of the fault. Decisions will be made based on the identified fault.

Reference [44] pointed out that fault isolation and identification are usually referred to as fault diagnosis. Fault diagnosis is very important for keeping the dynamic system robust and stable.

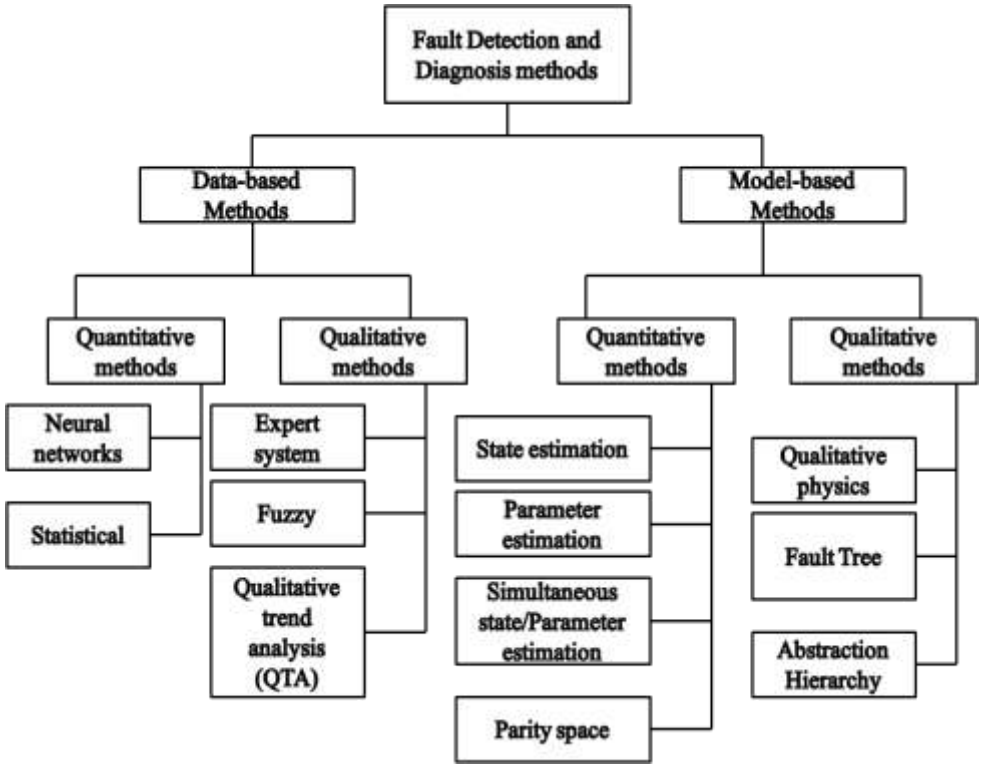

Figure 1-4 Classification of existing FDD methods

The existing FDD methodologies can be divided into model-based and data-based methods [3, 41, 42], as shown in Figure 1-4, based on the process knowledge that is required *a priori* [47]. The *a priori* is the relationship between observes and the faults. The *a priori* knowledge can be process history-based knowledge obtained from past experience with the process or it can be model-based knowledge developed from a fundamental understanding of the process using first-principle knowledge [48], such knowledge is referred as the model-based knowledge.

1.2.1 Model-based FDD schemes

The model-based FDD scheme has been studied widely since 1970s. On contrast to the data-based methods, the model-based FDD scheme utilizes the dependencies between

different measurable signals of the system to detect fault in the process, the actuators and the sensors. These dependencies are expressed by a mathematical model (often known as analytical redundancy) of a system especially the post-fault mathematical model to carry out FDD in real-time. The model-based FDD can also be divided into model-based quantitative FDD and model-based qualitative FDD, based on the definition of model. The model is described in mathematical functional relationships between inputs and outputs of the system in model-based quantitative models. In the model-based qualitative models, the model is expressed in terms of qualitative functions centered on different units in a process [41]. The qualitative models can be causal models or abstraction hierarchies. The qualitative models normally are used in analyzing the system reliability and safety.

1.2.1.1 Quantitative model-based FDD schemes

Various approaches to the FDD using quantitative model-based models have been reported in the last three decades. The basic structure of quantitative model-based FDD is based on the measured input and output signals. The detection methods generate residuals which reflect the discrepancy between the actual behavior of the system and the expected behavior given by its model. In a system working properly, the residual should be zero theoretically, which means there is no fault occurred in the system, and the residual should be above zero once faults occur in the system. Therefore, the residuals contain the information of faults. Decision functions are on the basis of the residual. The general procedure of quantitative model-based FDD is shown in Figure 1-5.

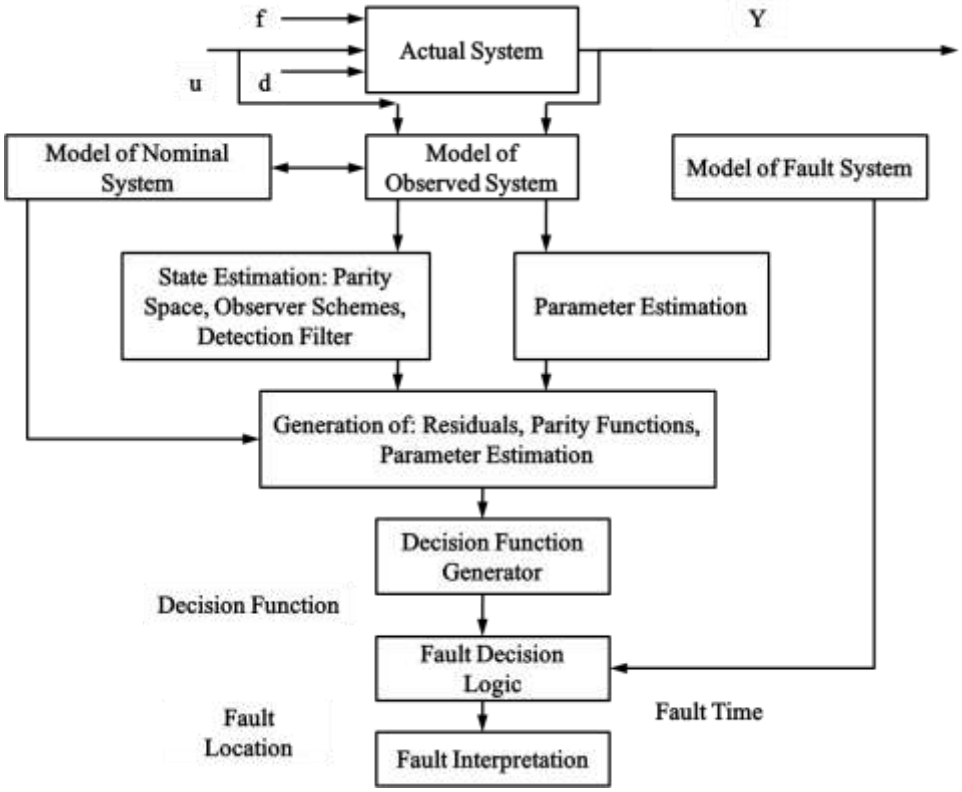

Figure 1-5 The procedure of FDD [6]

In Figure 1-5, *u* denotes the measured input, *f* denotes the fault occurred in the system, *d* represents the disturbance in the system and *Y* denotes the output signal of the system. The procedure of FDD can be divided into two steps:

1) Generation of a set of residuals;
2) Decision and isolation of the faults (time, location and magnitude).

Four main classes of model-based residual generators exist:

1) **Observer-based approach**, which reconstructs the output of the system from the measurements or a subset of the measurements with the aid of observers.

The difference between the measured outputs and the estimated outputs is used as the vector of residuals [17];

2) **Kalman filters method**, which is recursive algorithms for state estimation based on the system model in their normal operating modes. In this method, the filter gain is time-variant and linearized around the current operating point [41];
3) **Parity-space approach**, which checks the consistency of the mathematical equations of the system with the measurements [17]. A fault is detected when pre-assigned error bounds are surpassed. Since residuals are computed using measurements directly, the approach is very sensitive to measurement noise and system disturbances;
4) **Parameter estimation scheme**, which is based on the fact that faults of a dynamic system are reflected in the changes of physical parameters in the system. The idea of the parameter identification approach is to detect the faults via estimation of the parameters of the mathematical model. Parameter estimation schemes provide a means of the predicted system parameters online in real time and provide reference for controller reconfiguration [18].

If the parameters of the dynamic system are known, a FDD with observer-based approach and Kalman filter can be applied. However, in most practical situations the parameters are not known or only partially known, hence the parameter estimation approach can be applied.

The parameter estimation approach has three main attributions: detects and diagnoses as soon as possible, identifies the fault precisely and satisfies the requirements of

controller reconfiguration unit. In Section 3.1, parameter estimation will be discussed in more details. There are two approaches of parameter estimation: One is the direct estimation of the parameters, which can be applied when the parameters are linear. In this case, the well-known least squares (LS) estimation methodology can be used. The second approach is Kalman filter algorithm, which is applied widely when the iterative procedure is needed under the influence of the process disturbances.

1.2.1.2 Qualitative model-based FDD schemes

For the sake of brevity, only some of many techniques will be introduced in this section, they are *fault trees, qualitative physics classes*, and *digraphs* approaches.

1) **Qualitative physics**, which has been used in the artificial intelligence area. Its knowledge can be represented in two ways: One is to model the generic behavior of the system based on qualitative differential equations termed as confluences equations and qualitative state [51, 52], and the other is to derive qualitative equations from the ordinary differential equations [52, 54]. The advantage of qualitative physics approach is that it determines all of the behaviors of the system without an accurate mathematical model [41], but the drawback is deriving confluence equations could be ambiguous and spurious;
2) **Fault tree analysis (FTA)**, which was developed at Bell Telephone Laboratories in 1961. It consists layers of nodes which use logic operations such as AND, OR and XOR to transmit primary events or faults to top level event. Fault trees are mainly used in system reliability analysis [41];
3) **Digraph-based approach**, which uses signed digraphs (SDG) to describe cause-effect relation or model. Each node of SDG represents an event or a

variable, and the edge means the relationship between the nodes. SDG uses the directed arcs to describe the change between the nodes. SDGs provide a visual and direct way of describing the model, and have been widely used in process fault diagnosis [41].

1.2.2 Data-based FDD schemes

Data-based FDD method is the traditional approach to FDD. It is primarily based on large amount of historical process data. Data-based FDD method has two branches which are qualitative and quantitative depending on the implementation of feature extraction processing which is to transform and present data as *a priori* knowledge to a diagnostic system [42].

1.2.2.1 Qualitative data-based FDD schemes

Two popular methods that use qualitative feature extraction are the *expert system* and *qualitative trend analysis* approaches.

1) **Expert system**, which is defined by Feigenbaum [45] as "an intelligent computer program that uses knowledge and inference procedures to solve problems that are difficult enough to require significant human expertise for their solution". A large number of methods of expert system have been developed since 1984. The earliest application of expert systems for FDD was for a whipped topping process [42]. The advantage of an expert system method is its easy for implementation, efficiency and effectiveness, but the limitation of an expert system approach is that it is difficult to update and very system-specific;

2) **Qualitative trend analysis (QTA)**, which utilizes the trend information presented in sensor measurements via two basic steps which are identification of trends in measurements and interpretation of trends in terms of fault scenarios. A large number of methods have been developed for the representation of the process trends, such as triangulation finite difference method, a neural network based extraction of primitive trends, a wavelet theory based adaptive trend analysis, a dyadic B-splines based trend analysis algorithm, etc [42].

1.2.2.2 Quantitative data-based FDD schemes

In the development of quantitative feature extraction, the diagnostic problem-solving is regarded as a pattern recognition problem. Two popular methods that use quantitative feature extraction are the *statistical process control* and *neural networks based* approaches.

1) **Statistical process control (SPC),** which includes univariate SPC (USPC) and multivariate SPC (MSPC). The USPC is less efficient than the MSPC and it cannot provide complete information about the interactions between variables. The MSPC is to transform a number of related process variables to a smaller set of uncorrelated variables [42]. Principal component analysis (PCA) and partial least squares (PLS) methods as the members of MSPC have been applied widely. The PCA and PLS do not need an exact system model. The drawback of MSPC is that it is limited to linear additive faults and it cannot recognize the fault isolation;

2) **Neural networks (NN) based methods,** which can be classified into the architecture of the neural network and the learning strategy. The NN has been extensively applied since 1988. The most popular processing algorithms are back-propagation algorithm, self-organizing maps, ART2 network, and K-mean clustering algorithm. The limitations of NN are that it is only based on historic process data, it cannot generalize to unknown regions of measurements space and it cannot handle multiple faults [42].

In general, the drawback of data-based method is that sampling the distribution of a class of data in the measurement space has strong implication on the results. It does not consider the interrelationship of measured signals of the system. Hence, data-based method is not adopted in this thesis work.

1.3 Proposed Fault Detection and Diagnosis Schemes

There are two FDD schemes implemented in this thesis work. Both of them belong to model-based FDD scheme. One is Adaptive Two-Stage Extended Kalman Filter (ATSEKF), which is for estimating the amount of actuator effectiveness reduction. The ATSEKF can be used to estimate the changes of biased parameters which model the faults in nonlinear system. However, in ATSEKF, it has to do system linearization around the equilibrium point at each step. So it makes the implementation difficult if the system has complex mathematical model.

For estimation to nonlinear systems, the conventional EKF has been applied widely. However, Unscented Kalman Filter (UKF) has drawn significant research recently for state estimation applications due to its unique feature without a need for system

linearization at each time step as required by EKF [23]. The EKF is the nonlinear version of the Kalman filter, and it only simply linearizes about the current mean and covariance. Hence, the EKF can only preserve the first-order system statistics and may quickly diverge if the process is not modeled correctly, due to the modeling errors generated through linearization operation. The UKF is the improvement of the EKF to replace it in nonlinear filtering problems. In the UKF, the probability density is approximated by the nonlinear transformation of a random variable, which returns much more accurate results than the first-order Taylor expansion of the nonlinear functions used in the EKF. The approximation utilizes a set of sample points, referred to as *sigma points*, which guarantees accuracy with the posterior mean and covariance to the second order for any nonlinearity [39].

In this thesis work, both the system state variables and the actuator fault parameters are estimated by using ATSEKF and Dual Unscented Kalman filter (DUKF) in the FDD module. DUKF is an extension of the UKF for providing simultaneous system states and fault parameters estimation for the purpose of application to FDD. In Chapter 3, the ATSEKF and the DUKF will be discussed in details.

1.4 Objectives

This thesis addresses two FDD schemes implemented on three aircraft benchmarks which are a quad-rotor helicopter UAV (Unmanned Aerial Vehicle), a NASA fixed-wing UAV model referred to as Generic Transport Model (GTM) and a Boeing 747 series 100/200 airplane based on the measured outputs of the sensors and the inputs to actuators (i.e. controller outputs). The unpredicted fault considered in this thesis is the actuator

partial loss. Joint/simultaneous state and parameter estimation is chosen as FDD scheme since it can provide sufficient information for controller reconfiguration which will be discussed in Chapter 3 in details. Two different Kalman filter algorithms which are ATSEKF and DUKF are used as joint state and parameter estimation scheme for the purpose of FDD of both fixed-wing and rotary-wing UAVs in the presence of partial loss faults in actuators.

The main contributions of this research are as follows:

1) Develop the ATSEKF and DUKF schemes for FDD of the quad-rotor UAV, GTM and Boeing 747 models;
2) Simulate various partial losses on actuator control effectiveness to validate the performance of the ATSEKF and DUKF;
3) Evaluate and compare the performance of the ATSEKF and DUKF in both linearized environment and high-fidelity nonlinear environment through simulations under three aircraft models.

1.5 Outline of the Thesis

This thesis includes six chapters. Chapter 1 presents the motivation of FDD, literature review of model-based FDD and data-based FDD and the proposed FDD schemes in this thesis. Chapter 2 starts with the definition of types of faults and modeling with actuator faults, sensors faults and components faults. Chapter 2 ends with presentation of formulation of actuator faults. In Chapter 3, FDD methodologies are introduced in detail. Chapter 4 presents three different aircraft benchmarks which are a quad-rotor UAV, a

fixed-wing UAV model of the NASA GTM and a Boeing 747 series 100/200 airplane. In Chapter 5, simulation results demonstrate that model-based FDD approaches depend on the accurate mathematical model of the dynamic system. Finally conclusions and future works are discussed in Chapter 6.

2 Fault/Failure Classification

To achieve high control performance, an AFTCS relies on real-time FDD to provide precise information on faults in the system. Therefore, for a high performance FTCS, when a fault/failure occurs either in an actuator, sensor or plant, a FDD scheme will detect and diagnose the source and the magnitude of the fault. The reconfiguration scheme will design the reconfigurable controller based on this information to balance and adapt to the faults and failures.

This chapter will start from the definition of fault and failure. Later, it will explain three types of fault, and give the formulation of actuator faults.

2.1 Definition of fault/failure

Fault: an undesired change in a system parameter that degrades performance and a fault may not represent a component failure [62].

Failure: a catastrophic or complete breakdown of a component or function (to be contrasted with a fault which may be a tolerable malfunction) [62].

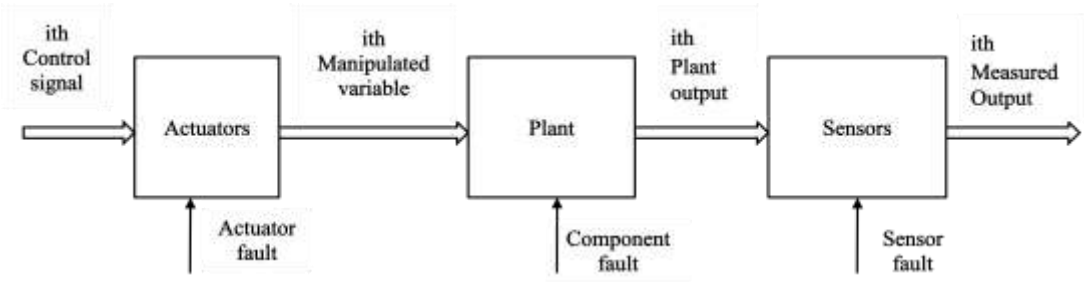

Figure 2-1 Block diagram of fault position

With respect to the location where the faults take place as shown in Figure 2-1, faults can be classified into three types: actuator faults, sensors faults and component faults. Generally speaking, when a fault occurs in the system, such as an actuator, the system performance may be degraded, but it may still be controllable. While when a failure occurs, the system maybe be crushed and lose the control completely. Therefore, a failure is much more severe than a fault based on the above definition.

2.2 Types of faults

2.2.1 Actuator faults

An actuator is a mechanical device which converts external energy into needed motion, and it is a necessary component in any control systems and has been widely used in industrial applications and manufacturing. Actuator faults are widely researched in aerospace industry. In this thesis, only this kind of faults is discussed.

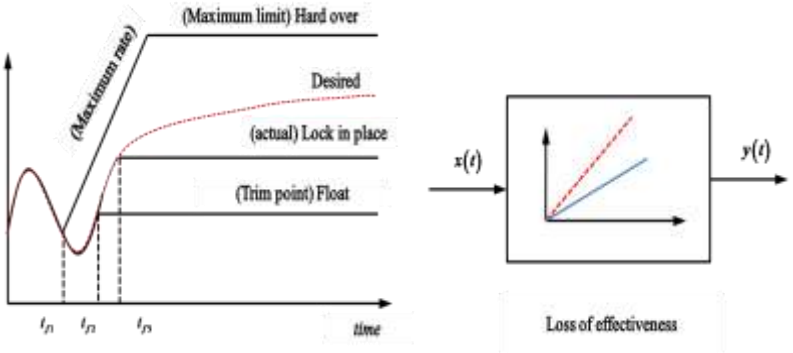

Figure 2-2 Types of actuator faults

The classification of actuator faults depends on the types of actuators, but generally faults in actuators can be divided into four types: a) lock in place failure, also called as

stuck failure; b) float failure; c) hard over failure, and d) partial loss of effectiveness fault. Figure 2-2 depicts the above faults occurring in actuators.

Lock in place failure occurs when the actuator is stuck/frozen at certain position or has no response to the control input. Float failure occurs when the actuator moves freely without providing any force/moment to the aircraft and does not contribute to the control authority. Hard over failure is defined as any failure of the flight control system which causes a rapid and sustained displacement of an aircraft aerodynamic control surface to the full extent permitted by physical constraints within the actuation system [16]. Partial loss of actuator control effectiveness occurs when the efficiency of one or multiple actuators reduces. The consequences of actuator faults may be very dangerous, especially for the aircraft. Some actuator faults cause low efficiency, high consumption of actuators, while some result in the partial or total loss of control. In this thesis, partial loss of control effectiveness is considered.

2.2.2 Sensor faults

A sensor is a device which receives and measures signals of a system's internal states, and it then converts them into corresponding signal outputs which can be used by external world.

Faults in sensors usually can be divided into five categories: 1) bias failure; 2) drift failure; 3) loss of accuracy failure; 4) freezing and 5) calibration error. Figure 2-3 depicts the above faults occurring in sensors.

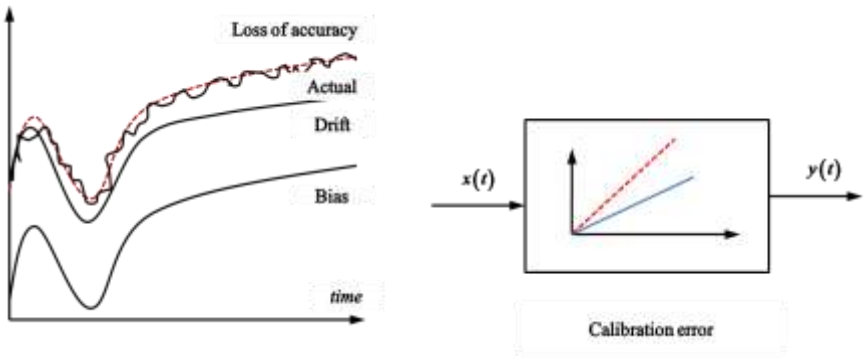

Figure 2-3 Types of sensors faults

Bias failure is a constant offset/error between the actual and measured signals. The sensor drift failure is a condition whereby the measurement errors increase over time. The loss of accuracy occurs when the measurements never reflect the true values of the physical variables. Freezing of sensor signals indicates that the sensor provides a constant value instead of the true value. Finally the calibration error is a wrong representation of the actual physical meaning of the states from the electrical or electronic signals that come out from the sensor unit itself.

2.2.3 Component faults

The components faults shown in Figure 2-4 are modeled by any change in the parameter θ in the system making the nominal model of the dynamic system invalid. It affects the input-output state-space model in a multiplicative manner as shown in Figure 2-5.

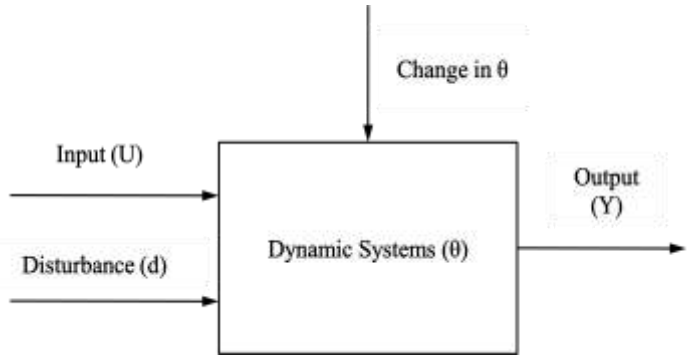

Figure 2-4 Model of component faults

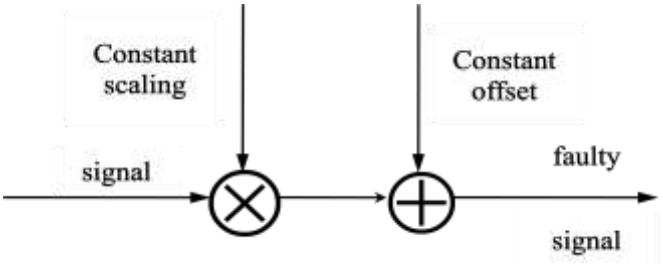

Figure 2-5 Multiplicative faults [63]

2.3 Formulation of actuator faults

An actuator fault can be normally represented in the reduction of the actuator's effectiveness. A linear time-varying system associated with the actuator faults can be represented by following equations:

$$\dot{x}(t) = Ax(t) + Bu(t) - B\gamma u(t) + w(t) \tag{2.1}$$

$$y(t) = Cx(t) + v(t) \tag{2.2}$$

where $x(t) \in \mathbb{R}^n$, $u(t) \in \mathbb{R}^l$ and $y(t) \in \mathbb{R}^l$ are the system state, control input and system output variables, respectively. $w(t)$ and $v(t)$ denote white noises. $\gamma = diag(\gamma_1, \ldots, \gamma_m)$

where γ_i are scalars satisfying $0 \le \gamma_i \le 1$. If $\gamma_i = 0$, the i_{th} actuator is working perfectly whereas if $\gamma_i \ge 0$, a fault is present, and if $\gamma_i = 1$, the actuator has failed completely. The Equation (2.1) represents a partial loss in the effectiveness via γ_i. By the formula, it can be discovered that faults are related to the aircraft's control surfaces. The objective of FDD is to determine the extent of the loss in the control effectiveness γ_i.

But considering the effects of faults/failures only in the B matrix of the linear system is not sufficient. Structural damage could also happen during the flight and it will change the aerodynamic coefficients/derivatives of the aircraft or the centre of gravity, and therefore it may change the operating conditions of the aircraft from its nominal conditions. In terms of linear control systems, the A matrix will also be perturbed. This can be represented as:

$$\dot{x}(t) = (A + \Delta A)x(t) + (B + \Delta B)u(t) + w(t) \tag{2.3}$$

where ΔA and ΔB represent the changes in the A and B matrices. Examples of failures that cause structural damage are wing battle damage, and detachment of control surfaces [38]. In this thesis work, however, only the changes in B matrix are considered.

2.4 Summary

This chapter has stated briefly the definition of a fault and a failure, discussed the type of faults/failures based on the location where faults/failures will occur. Mathematical formulation of actuator faults in terms of partial loss of actuator control effectiveness is also presented in this chapter.

3 FDD Schemes Developed in This Thesis

Joint state and parameter estimation schemes for FDD are adopted in this thesis. This chapter will start with presentation of the concept and procedure of parameter estimation. Then the ATSEKF and DUKF algorithms for simultaneous states and fault parameters estimation are presented.

In general, a set of equations of motion can be used to describe the motion of a flight vehicle, and parameters can keep constant over the period of observation. However, when an actuator fault happens, for example a stuck failure in rudder, spoiler or elevator or partial loss of its effectiveness, the parameters of the aircraft system will deviate from their normal values. Aircraft model contains a great number of coefficients, especially aerodynamic coefficients and derivatives, which could change when the operating conditions change or faults occur. These coefficients are obtained offline by performing thousands of experiments through wind tunnel and/or flight tests before being used for modeling or control design. However, compared with online parameter estimation, the offline estimate is not accurate and cannot be quite synonymous with controllers in the presence of fault/damage. Parameter estimation technique has been applied to aircraft to determine aerodynamic coefficients and derivatives [38].

3.1 Parameter estimation

The main concept of the parameter estimation methods for FDD is that faults are associated with the physical coefficients of the process. The parameter estimation

approaches make use of deviations in the model parameters during detecting and isolating faults. For parameter estimation, the residuals are the difference between the nominal and the estimated model parameters. In a system working properly, the residual should be zero theoretically, which means there is no fault occurred in the system, and the residual should be above zero once faults occur in the system. By estimating the parameters of a process model on-line, residuals are computed as the parameter estimation errors and will be passed to the reconfiguration controller. To successfully diagnose faults/failures, the mapping from the model coefficients to the process parameters is necessary.

Consider the following mathematical model of a dynamic system:

$$y(t) = f(u, w, \gamma, t) \tag{3.1}$$

where $u(t)$ represents the input of the system, $y(t)$ is the output vector, $w(t)$ represents the noise vector, and γ denotes the parameters vector which is associated with the faults.

The idea of the parameter identification approach is to detect the faults via estimated parameters of the mathematical model based on the following procedure shown in Figure 3-1:

Step 1: Choice of a parametric model of the system, $y(t) = f(u, \gamma, t)$;

Step 2: Determination of the relationships between the model parameters, γ_i and the physical parameters p_i;

Step 3: Identification of the model parameter vector γ using the input $u(t)$ and output $y(t)$ of the actual system (or of a system component);

Step 4: Determination of the physical parameter vector $p(t) = f^{-1}(\hat{\gamma}(t))$;

Step 5: Calculation of the vector of deviations, Δp, from its nominal value taken from the nominal model;

Step 6: Decision on a fault by exploiting the relationship between faults and changes in the physical parameters.

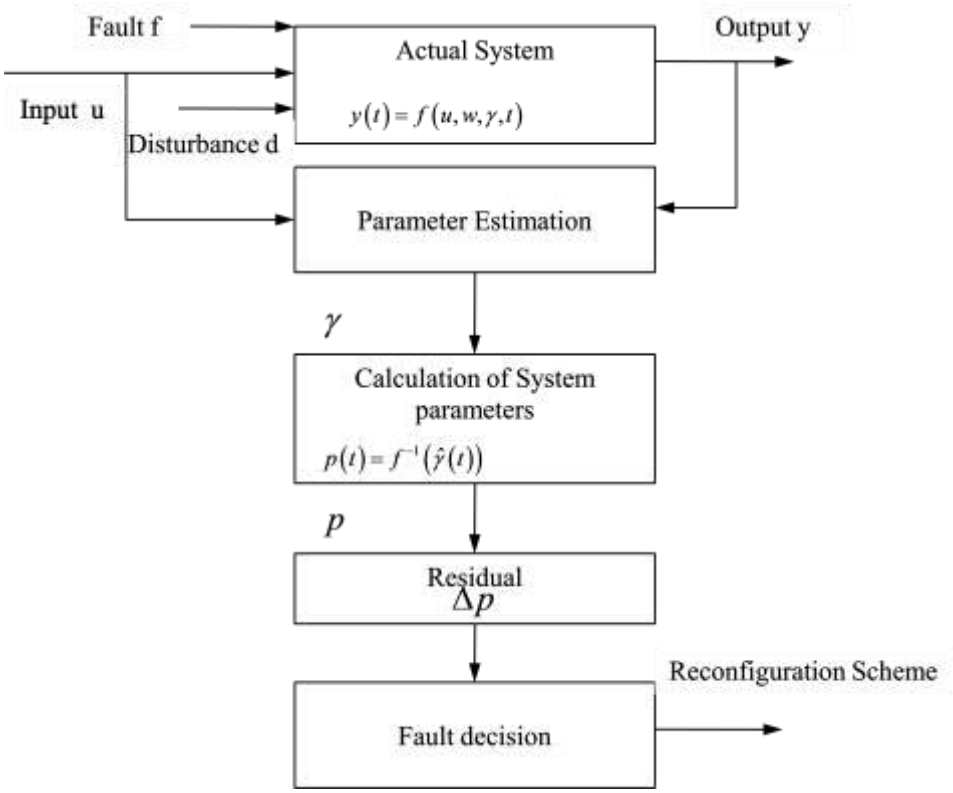

Figure 3-1 Procedure of parameter estimation

Hence, by augmenting the system state vector by artificially defining the unknown parameters θ as additional state variables, parameter estimation is achieved. Therefore, parameter estimation is transformed into state estimation.

In Equation (2.1), $\gamma = diag(\gamma_1, \ldots, \gamma_m)$ where γ_i are scalars satisfying $0 \le \gamma_i \le 1$, and can also be used as fault detection parameter vector. In this thesis work, this scheme is the same for both ATSEKF and DUKF.

Different parameter estimation methods for FDD have been explored like extended Kalman filter, two-step method and least squares estimation [41]. In this thesis, ATSEKF and DUKF are implemented in three aircraft dynamic models which fall into a framework of joint/simultaneous state and parameter estimation scheme.

In this work, both the system state variables and the actuator fault parameters are estimated by using an ATSEKF scheme and a DUKF algorithm in the FDD module. In this chapter, the ATSEKF and DUKF algorithms are presented in detail after the conventional Kalman filter is elaborated.

3.2 The Kalman filter

The Kalman filter is an efficient recursive filter that estimates the state of a linear dynamic system from a series of noisy measurements [9]. Theoretically, the Kalman filter is an estimator for so-called linear-quadratic problem, which is the problem of estimating the instantaneous states of a linear dynamic system perturbed by white noise using the measurements linearly related to the state and corrupted by white noise [10]. As a typical efficient recursive filter, the Kalman filter is often used to estimate the states of a dynamic system under white noise disturbances. The common applications include inertial navigation, sensor calibration, radar tracking, manufacturing, economics, signal processing, and freeway traffic modeling. The Kalman filter can be applied to both linear

and nonlinear systems. The extension of Kalman filter to handle nonlinear system is referred as to Extended Kalman Filter (EKF).

Consider a linear discrete-time system which is represented by two equations as follows:

$$x_{k+1} = F_{k+1,k} x_k + w_k \tag{3.2}$$

$$y_k = H_k x_k + v_k \tag{3.3}$$

The state vector, denoted by x_k, is defined as the minimal set of data that is sufficient to uniquely describe the unforced dynamical behaviour of the system; the subscript *k* denotes discrete time. A set of observed data, denoted by the vector y_k are used to estimate the state x_k. $F_{k+1,k}$ is the transition matrix taking the state x_k from time *k* to time *k+1*. y_k is the observable at time *k* and H_k is the measurement matrix. The process noise w_k and the measurement noise v_k are assumed to be additive, white, and Gaussian, with zero mean and normal probability distributions.

$$p(w) \sim N(0, Q) \tag{3.4}$$

$$p(v) \sim N(0, R) \tag{3.5}$$

where *Q* is the process noise covariance matrix and *R* is the measurement noise covariance matrix.

The Kalman filter iterates between two steps:

1) **Time Update (Predict)**, the filter produces a time update at the current time step, based on the previous estimated states before obtaining any new measurements at the next time step using the system model;
2) **Measurement Update (Correct)**, once the new measurements information arrives at the new time step, the filter will produce more accurate state estimate. This is very close to the true value by combining the new measurements information with the result generated in the previous time update procedure based on an optimal adjustment.

Table 3-1 The Kalman filter algorithm

Initial Estimates: *For k = 0*

$$\hat{x}_0 = E(x_0)$$

$$P_0 = E\left[(x_0 - \hat{x}_0)(x_0 - \hat{x}_0)^T\right]$$

Time Update: *For k = 1, 2, …*

State estimation propagation:

$$\hat{x}_k = F_{k,k-1}\hat{x}_{k-1}^-$$

Error covariance propagation:

$$P_k^- = F_{k,k-1}P_{k-1}F_{k,k-1}^T + Q_{k-1}$$

Measurement Update: *For k = 1, 2, …*

Compute the Kalman gain matrix:

$$K_k = P_k^- H_k^T \left(H_k P_k^- H_k^T + R_k\right)^{-1}$$

Update state estimate:

$$\hat{x}_k = \hat{x}_k^- + K_k\left(y_k - H_k\hat{x}_k^-\right)$$

Update the error covariance:

$$P_k = (I - K_k H)P_k^-$$

where $\hat{x}_k^- \in R^n$ is defined as *a priori* state estimate at step k given knowledge of the process prior to step k and $\hat{x}_k \in R^n$ is defined as *a posteriori* state estimate at step k given measurement y_k. P_k^- is the *a priori* estimate error covariance. P_k is the *a posteriori*

estimate error covariance. $K_k \in R^{n\times m}$ is the Kalman gain that minimizes the *a posteriori* and *a priori* estimate errors covariance. This two-step recursion is applied at each successive time period. The Kalman filter cycle starts with the initial estimate of $\hat{x}_0$ and error covariance P_0. The time update step updates the current state and error covariance estimate *priori* time. The measurement calculates the Kalman gain K_k based on the *a priori* estimate error covariance P_k^-, and it is used to adjust the *a priori* state estimate $\hat{x}_k$ using the actual measurement y_k.

3.3 Extended Kalman filter

Generally, the Kalman filter is widely applied to estimate a value when it is measured in noisy environments, to predict time-varying variables based on a linear state-space model and using previous measurements and to obtain a value that is closest to the true value from more than one source with different types of sensor. The drawback of the conventional Kalman filter is that the estimated system has to be linear system. However, most physical systems are nonlinear and dynamic. Therefore, the Extend Kalman filter (EKF) was proposed to address this issue. The EKF extends the use of Kalman filter through a linearization procedure.

Consider a nonlinear dynamical system described by the state-space model:

$$\begin{aligned} x_{k+1} &= f\left(k, x_k\right) + w_k \\ y_k &= h\left(k, x_k\right) + v_k \end{aligned} \tag{3.6}$$

where w_k and v_k are independent, zero-mean, Gaussian noise processes of covariance matrices Q_k and R_k, respectively. The functional $f(k, x_k)$ denotes a nonlinear time-variant transition matrix function, and the functional $h(k, x_k)$ denotes a nonlinear time-variant measurement matrix. The EKF is to linearize the state model of Equation (3.6) at each step time around the most recent state estimation, which is taken to be either $\hat{x}_k$ or $\hat{x}_k^-$. The standard Kalman filter equations are applied, once a linear model is obtained.

$$F_{k,k-1} = \left.\frac{\partial f(k,x)}{\partial x}\right|_{x=\hat{x}_{k-1}}, \qquad H_k = \left.\frac{\partial h(k,x)}{\partial x}\right|_{x=\hat{x}_k^-} \tag{3.7}$$

Table 3-2 The extended Kalman filter algorithm

Initial Estimates: *For k = 0*

$$\hat{x}_0 = E[x_0]$$

$$P_0 = E\left[(x_0 - E[x_0])(x_0 - E[x_0])^T\right]$$

Time Update: *For k = 1, 2, …*

State estimation propagation:

$$\hat{x}_k^- = f(k, \hat{x}_{k-1})$$

Error covariance propagation:

$$P_k^- = F_{k,k-1} P_{k-1} F_{k,k-1}^T + Q_{k-1}$$

Measurement Update: *For k = 1, 2, …*

Compute the Kalman gain matrix:

$$K_k = P_k^- H_k^T \left[H_k P_k^- H_k^T + R_k\right]^{-1}$$

Update state estimate:

$$\hat{x}_k = \hat{x}_k^- + K_k y_k - h(k, \hat{x}_k^-)$$

Update the error covariance:

$$P_k = (I - K_k H_k) P_k^-$$

where $\hat{x}_k^- \in R^n$ is defined as *a priori* state estimate at step k given knowledge of the process prior to step k and $\hat{x}_k \in R^n$ is defined as *a posteriori* state estimate at step k given measurement y_k. P_k^- is the *a priori* estimate error covariance. P_k is the *a posteriori* estimate error covariance. $K_k \in R^{n \times m}$ is the Kalman gain that minimizes the *a posteriori* and *a priori* estimate errors covariance. This two-step recursion is applied at each successive time period. The EKF cycle starts with the initial estimate of $\hat{x}_0$ and error covariance P_0. At each time update step, EKF linearizes the state model by using Equation (3.7) for performing error covariance propagation, and updates the current state and error covariance estimate *priori* time. The measurement calculates the Kalman gain K_k based on the *a priori* estimate error covariance P_k^-, and it is used to adjust the *a priori* state estimate $\hat{x}_k^-$ for obtaining the *a posteriori* state estimate $\hat{x}_k$ using the actual measurement y_k.

3.4 The Adaptive Two-Stage Extended Kalman Filter (ATSEKF) Algorithm

The conventional Kalman filter can only be applied on the premise that complete and accurate system parameters is known and stochastic properties of noises is known as well, but in most cases, it is hard to obtain the accurate system model without any bias. Based on this fact, Friedland put forward a new procedure of separating the estimation of the unknown constant bias variables from the dynamic variables in 1969 [59]. This technique has been extensively studied and developed. In 1996, the pseudo separated-bias estimation (PSBE) algorithm was proposed by Zhang *et al* [58]. In 1997, an optimal

solution of the two-stage Kalman filter for linear stochastic systems subject to random bias was proposed by Keller and Darouach [56], and Wu and Zhang proposed the linear adaptive two-stage Kalman filter in 1998 [15].

3.4.1 The two-stage extended Kalman filter algorithm

This section introduces the nonlinear adaptive two-stage Kalman filter developed by Zhang *et al* [18] which is the extended version of the linear adaptive two-stage Kalman filter [15].

Consider a biased augmented nonlinear discrete-time system [18, 19]:

$$x(k+1) = f\left(x(k)\right) + G(k)u(k) + B_1(k)b(k) + w^x(k) \tag{3.8}$$

$$B_1(k) = G(k)U_k \tag{3.9}$$

where

$$U_k = \begin{bmatrix} u_k^1 & 0 & \cdots & 0 \\ 0 & u_k^2 & \ddots & 0 \\ 0 & \ddots & \ddots & \vdots \\ 0 & 0 & \cdots & u_k^l \end{bmatrix} \tag{3.10}$$

$$b(k+1) = b(k) + w^b \tag{3.11}$$

$$y(k+1) = h\left(x(k+1)\right) + B_2(k+1)b(k+1) + v(k+1) \tag{3.12}$$

where $x(k) \in R^n, b(k) \in R^q, u(k) \in R^l$ and $y(k+1) \in R^m$ are the state, bias, control input and output variables, respectively. $w^x(k), w^b(k)$ and $v(k+1)$ are the white noise

sequences of uncorrelated Gaussian random vectors with zero means and covariance matrices $Q^x(k) > 0, Q^b(k) > 0$ and $R(k+1) > 0$, respectively. The initial state $x(0)$ and bias $b(0)$ are assumed to be uncorrelated with the noise process $w^x(k), w^b(k)$ and $v(k+1)$. The initial state $x(0)$ and bias $b(0)$ are specified as random Gaussian vector with mean $\bar{x}_0$ and covariance $\bar{P}_0^x$, and mean $\bar{b}_0$ and covariance P_0^b, respectively. Figure 3-2 illustrates the signal flow of the TSEKF. The control signals *u* and measured outputs *z* are inputted into fault-free state estimator, the outputs of fault-free state estimator are coupled with the outputs of fault estimator $\hat{\gamma}$ via coupling equations, and the coupled results $\tilde{x}$ are compensated and generate the final results $\hat{x}$ of TSEKF.

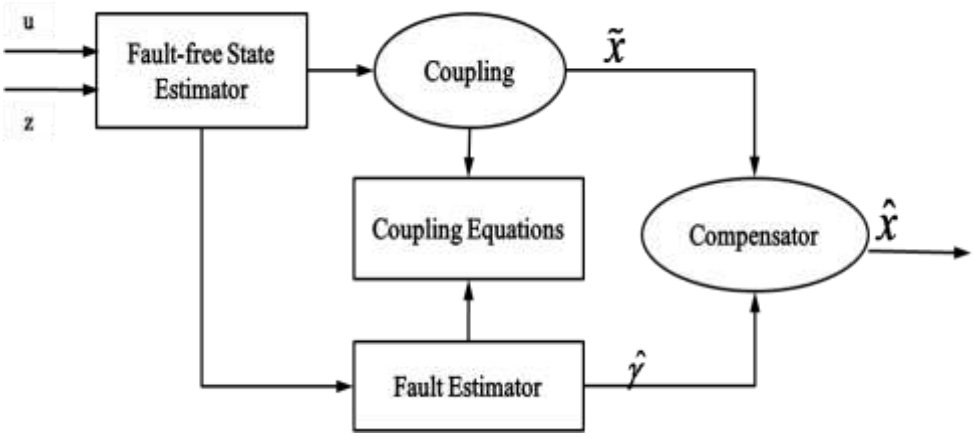

Figure 3-2 The signal flow of the TSEKF [1]

Fault-free state estimator:

$$\tilde{x}(k+1|k) = f\left[\tilde{x}(k|k)\right] + G(k)u(k) + \left[M(k) - V(k+1|k)\right]\hat{b}(k|k) \tag{3.13}$$

$$\begin{aligned}\tilde{P}^x(k^+|k) = {} & F\left[\tilde{x}(k|k),k\right]\tilde{P}^x(k|k)F^T\left[\tilde{x}(k|k),k\right] + Q^x(k) + \\ & M(k)P^b(k|k)M^T(k) - V(k+1|k)P^b(k+1|k)MV^T(k+1|k)\end{aligned} \tag{3.14}$$

$$\tilde{x}(k+1|k+1)=\tilde{x}(k+1|k)+\tilde{K}^{x}(k+1)\left[y(k+1)-h\left(\tilde{x}(k+1|k)\right)\right] \tag{3.15}$$

$$\tilde{K}^{x}(k+1)=\tilde{P}^{x}(k+1|k)H^{T}(k+1)\left[H(k+1)\tilde{P}^{x}(k+1|k)+R(k+1)\right]^{-1} \tag{3.16}$$

$$\tilde{P}^{x}(k+1|k+1)=\left[I-\tilde{K}^{x}(k+1)H(k+1)\right]\tilde{P}^{x}(k+1|k) \tag{3.17}$$

where the filter residual vector and its covariance are given as

$$\bar{r}(k+1)=y(k+1)-h\left(\tilde{x}(k+1|k)\right) \tag{3.18}$$

$$\tilde{S}(k+1)=H(k+1)\tilde{P}(k+1|k)H^{T}(k+1)+R(k+1) \tag{3.19}$$

The Jacobians in the Taylor's series expansion for nonlinear function f and h are

$$\begin{aligned} F\left[\bar{x}(k|k),k\right] &= \frac{\partial f}{\partial x}|_{x=\tilde{x}(k|k)} \\ H(k+1) &= \frac{\partial h}{\partial x}|_{x=\tilde{x}(k+1|k)} \end{aligned} \tag{3.20}$$

Fault estimator:

$$\hat{b}(k+1|k)=\hat{b}(k|k) \tag{3.21}$$

$$P^{b}(k+1|k)=P^{b}(k|k)+Q^{b}(k) \tag{3.22}$$

$$\hat{b}(k+1|k+1)=\hat{b}(k+1|k)+K^{b}(k+1)\left[\tilde{r}(k+1)-N(k+1|k)\hat{b}(k|k)\right] \tag{3.23}$$

$$K^{b}(k+1)=P^{b}(k+1|k)N^{T}(k+1|k)\left[N(k+1|k)P^{b}(k+1|k)N^{T}(k+1|k)+\tilde{S}(k+1)\right]^{-1} \tag{3.24}$$

$$P^{b}(k+1|k+1)=\left[I-K^{b}(k+1)N(k+1|k)\right]P^{b}(k+1|k) \tag{3.25}$$

Coupling equations:

$$M(k) = F\left[\bar{x}(k|k), k\right] V(k|k) + B_1(k) \tag{3.26}$$

$$V(k+1|k) = M(k) P^b(k|k) \left[P^b(k+1|k)\right]^{-1} \tag{3.27}$$

$$N(k+1|k) = H(k+1) V(k+1|k) + B_2(k+1) \tag{3.28}$$

$$V(k+1|k+1) = V(k+1|k) - \tilde{K}^x(k+1) N(k+1|k) \tag{3.29}$$

Compensated state and error covariance estimates:

$$\tilde{x}(k+1|k+1) = \bar{x}(k+1|k+1) + V(k+1|k+1) \hat{b}(k+1|k+1) \tag{3.30}$$

$$P(k+1|k+1) = \tilde{P}^x(k+1|k+1) + V(k+1|k+1) P^b(k+1|k+1) V^T(k+1|k+1) \tag{3.31}$$

The modification made to the two-stage Kalman filter in [56] is by using time-varying matrices to replace the constant coefficient matrices.

3.4.2 The adaptive two-stage Extended Kalman filter algorithm

In order to response to abrupt changes in the control effectiveness factors, forgetting factors are adopted. The basic idea is to enable a recursive algorithm to discount the past information so that the filter is more apt to recognize the changes in the system [55], and therefore Equation (3.22) is modified to

$$P^b(k+1|k) = P^b(k|k)/\lambda + Q^b(k), \quad 0 < \lambda \leq 1 \tag{3.32}$$

where λ is a single constant forgetting factor. The adjusted covariance $P^b(k+1|k)$ should be within some prescribed bounds

$$\sigma_{\min} I \le P^b(k+1|k) \le \sigma_{\max} I \tag{3.33}$$

where $\sigma_{\min}$, $\sigma_{\max}$ are positive constant and I is the identity matrix, since covariance $P^b(k|k)$ cannot be too large or too small.

The dyadic expansion of $P^b(k|k)$ is

$$P^b(k|k) = \sum_{i=1}^{l} \alpha_{k|k}^i e_k^i \left(e_k^i\right)^T \tag{3.34}$$

where $\alpha_{k|k}^i$ is the eigenvalues of $P^b(k|k)$ with $\alpha_{k|k}^1 \ge \cdots \ge \alpha_{k|k}^l$, and $e_k^1 \cdots e_k^l$ are the corresponding eigenvectors with $\| e_k^1 \| = \cdots = \| e_k^l \| = 1$. Finally, Equation (3.21) is evolved into

$$P^b(k+1|k) = \sum_{i=1}^{p} \frac{\alpha_i(k|k)}{\lambda_i(k)} e_i(k) e_i^T(k) + Q^b(k), 0 < \lambda_i(k) \le 1 \tag{3.35}$$

The forgetting factor $\lambda_i(k)$ can be chosen as a decreasing function of the amount of information received in the direction $e_i(k)$. Since eigenvalue $\alpha_i(k|k)$ of $P^b(k+1|k)$ is a measure of the uncertainty in the direction of $e_i(k)$, a choice of forgetting factor $\lambda_i(k)$ can be

$$\lambda_i(k) = \begin{cases} 1, & \alpha_i(k|k) > \alpha_{\max} \\ \alpha_i(k|k)\left[\alpha_{\min} + \dfrac{\alpha_{\max} - \alpha_{\min}}{\alpha_{\max}} \alpha_i(k|k)\right]^{-1}, & \alpha_i(k|k) \le \alpha_{\max} \end{cases} \tag{3.36}$$

This forgetting factor ensures that Equation (3.32) can be satisfied. By replacing Equation (3.32) by Equations (3.35) and (3.36), the ATSEKF is realized eventually.

3.5 Dual Unscented Kalman Filter (DUKF) Algorithm

The EKF, including the ATSEKF, approximates the nonlinearities of the system's dynamics by linearizing the system at each time step through the first-order linearization of the nonlinear system. The EKF is a suboptimal nonlinear filter by truncating the higher order terms during linearization of the system [20]. The main drawbacks of the EKF are 1) easy to be divergent and be unstable; 2) difficult to implement the derivation of the Jacobian matrices; 3) convergence of parameters estimation is slow and even without guarantee of parameters convergence [21, 25]. In this case, the Unscented Kalman Filter (UKF) was proposed to overcome the shortcomings of the EKF [25]. The UKF is one of sigma-point Kalman filter which uses the statistical linearization technique. UKF is mainly used in nonlinear system identification, training of neural networks and dual estimation problems [20-22]. In this section, an overview of the DUKF state-parameter estimation scheme implemented for estimation of the loss of the actuator's effectiveness due to fault occurred in actuators is presented.

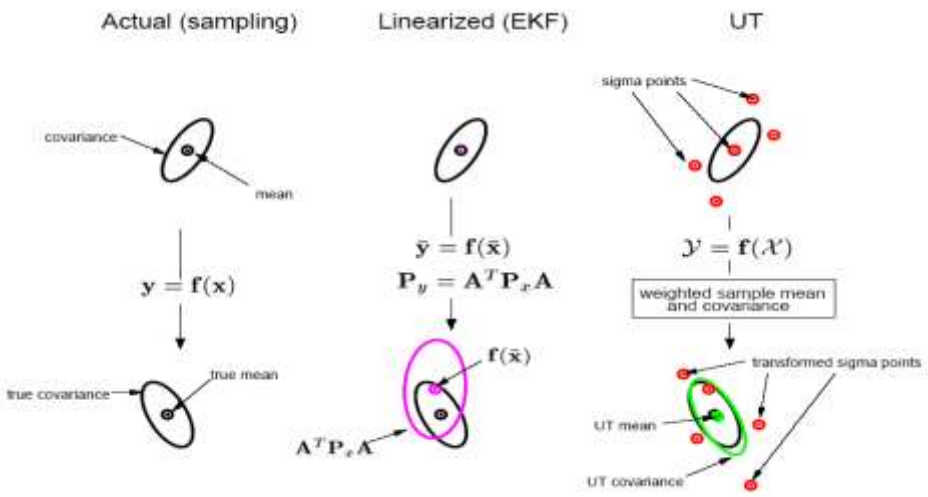

Figure 3-3 The unscented transfer for mean and covariance propagation [25]

For a highly non-linear model for estimation purpose, the UKF picks a minimal set of sample points which are called *sigma points* around the mean. These sigma points are then propagated through the non-linear functions and the covariance of the estimate is recovered [23]. These sigma points completely capture the true mean and covariance of the Gaussian random variables, and when propagated through the true nonlinear system, the *posterior* mean and covariance are accurately captured to the 3rd order (Taylor series expansion) for any nonlinearity [25]. Thus, the UKF captures both the first-order and second-order statistics of the nonlinear system through a so-called Unscented Transformation (UT), and hence has better estimation performance compared with EKF which only simply linearizes about the current mean and covariance with first-order statics as shown in Figure 3-3.

3.5.1 Unscented transformation

The unscented transformation (UT) proposed by Julier is a method for calculating the statistics of a random variable which undergoes a nonlinear transformation [24]. It is built on the principle that it is easier to approximate a probability distribution than an arbitrary nonlinear function [25].

Consider a nonlinear model $y = f(x)$, and the random variable x whose dimension is L, and assume x has mean $\bar{x}$ and covariance P_x. The basic steps of UT are:

1) Chose a set of points (sigma points) so that their sample mean and sample covariance are $\bar{x}$ and P_{x^-};
2) Apply each sigma point in turn to the nonlinear function to yield a cloud of transformed points and $\bar{y}$ and P_y are the statistics of the transformed points.

The L-dimensional random variable x with mean $\bar{x}$ and covariance $\bar{P}_x$ is approximated by $2L+1$ sigma points. In order to calculate the statistics of y, χ which is the matrix of $2L+1$ sigma vectors χ_i is formed.

$$\chi_0 = \bar{x} \tag{3.37}$$

$$\chi_i = \bar{x} + \left(\sqrt{(L+\lambda)P_x}\right)_i, \quad i = 1, \cdots, L \tag{3.38}$$

$$\chi_i = \bar{x} - \left(\sqrt{(L+\lambda)P_x}\right)_i, \quad i = L+1, \cdots, 2L \tag{3.39}$$

the weights for the state and covariance are given by:

$$\beta_0^{(m)} = \frac{\lambda}{L+\lambda} \tag{3.40}$$

$$\beta_0^{(c)} = \frac{\lambda}{L+\lambda} + \left(1-\alpha^2+\beta\right) \tag{3.41}$$

$$\beta_i^{(m)} = \beta_i^{(c)} = \frac{1}{\left[2\left(L+\lambda\right)\right]}, \quad i = 1,\cdots,2L \tag{3.42}$$

where $\lambda = \alpha^2\left(L+k\right)-L$ is a scaling parameter. α determines the spread of the sigma points around $\bar{x}$. The *k* is a secondary scaling parameter, and β is to incorporate prior knowledge of the distribution of *x*. $\left(\sqrt{\left(L+\lambda\right)P_x}\right)_i$ is the *i*th column of the matrix square root. In this thesis, α, β, and *k* are equal to 1, 2, and 3-*L*, respectively. χ_i is propagated through the nonlinear function

$$\psi_i = f\left(\chi_i\right), i = 0,\ldots,2L \tag{3.43}$$

$$\bar{y} \approx \sum_{i=0}^{2L} \beta_i^{(m)} \psi_i \tag{3.44}$$

$$P_y \approx \sum_{i=0}^{2L} \beta_i^{(c)} \left(\psi_i - \bar{y}\right)\left(\psi_i - \bar{y}\right)^T \tag{3.45}$$

where $\bar{y}$ is the mean for *y* and P_y is the covariance of the *posterior* sigma points. Figure 3-4 presents the implementation of UT.

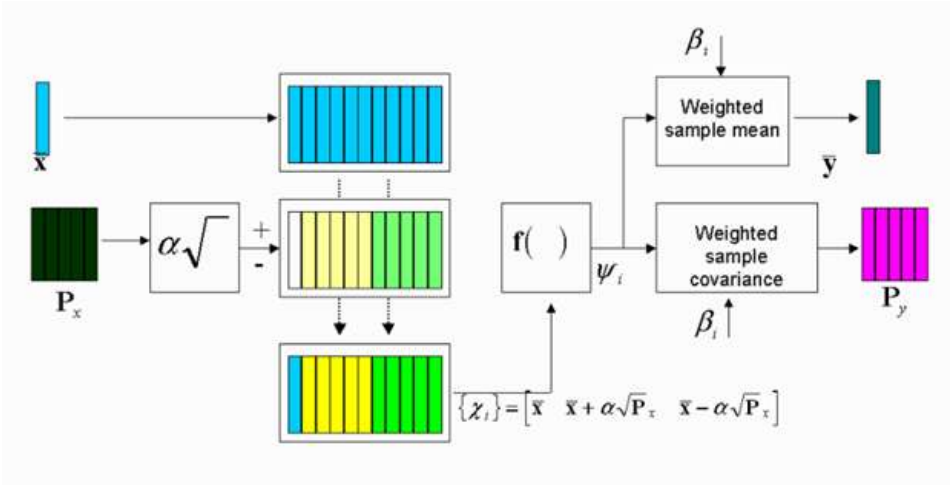

Figure 3-4 Unscented Transformation [12]

3.5.2 State estimation

Consider a nonlinear transform of a random variable: $y = f(x)$

Given: $\bar{x} = E[x]$, $P_x = E\left[(x-\bar{x})(x-\bar{x})^T\right]$

Find: $\bar{y} = E[y]$, $P_y = E\left[(y-\bar{y})(y-\bar{y})^T\right]$

A set of $2L+1$ sigma points is derived as following equations from the augmented state and covariance where L denotes the dimension of the augmented state.

$$\chi^0{}_{k-1|k-1} = \chi^\alpha{}_{k-1|k-1} \tag{3.46}$$

$$\chi^i{}_{k-1|k-1} = \chi^\alpha{}_{k-1|k-1} + \left(\sqrt{(L+\lambda)P^\alpha{}_{k-1|k-1}}\right)_i, \quad i = 1,\cdots,L \tag{3.47}$$

$$\chi^i{}_{k-1|k-1} = \chi^\alpha{}_{k-1|k-1} - \left(\sqrt{(L+\lambda)P^\alpha{}_{k-1|k-1}}\right)_i, \quad i = L+1,\cdots,2L \tag{3.48}$$

where $\left(\sqrt{(L+\lambda)P^{\alpha}{}_{k-1|k-1}}\right)_i$ is the *i*th column of the matrix square root of $\sqrt{(L+\lambda)P^{\alpha}{}_{k-1|k-1}}$ using the definition: square root A of matrix B satisfies $B \equiv AA^T$. χ is the matrix of 2*L*+1 sigma vectors.

The complete state estimation of the UKF is given in Table 3-3:

Table 3-3 The UKF state estimation algorithm

Initial estimates:

$$\hat{x}_0 = E\left[x_0\right]$$

$$\hat{x}_0^{\alpha} = E\left[x^{\alpha}\right] = \left[\hat{x}_0{}^T \quad 0 \quad 0\right]^T$$

$$P_0 = E\left[\left(x_0 - \hat{x}_0\right)\left(x_0 - \hat{x}_0\right)^T\right]$$

$$P_0^{\alpha} = E\left[\left(x_0^{\alpha} - \hat{x}_0^{\alpha}\right)\left(x_0^{\alpha} - \hat{x}_0^{\alpha}\right)^T\right] = \begin{bmatrix} P_0 & 0 & 0 \\ 0 & R^v & 0 \\ 0 & 0 & R^n \end{bmatrix}$$

Calculate the sigma points:

$$\chi_{k-1}^{\alpha} = \left[\hat{x}_{k-1}^{\alpha} \quad \hat{x}_{k-1}^{\alpha} + \gamma\sqrt{P_{k-1}^{\alpha}} \quad \hat{x}_{k-1}^{\alpha} - \gamma\sqrt{P_{k-1}^{\alpha}}\right]$$

$$k \in \{1, \cdots, \infty\}$$

Time update:

$$\chi_{k|k-1}^{x} = F\left(\chi_{k-1}^{x}, u_{k-1}, \chi_{k-1}^{v}\right)$$

$$\mathcal{Y}_{k|k-1} = H\left(\chi_{i,k|k-1}^{x}, \chi_{k-1}^{n}\right)$$

$$\hat{x}_k^- = \sum_{i=0}^{2L} \beta_i^{(m)} \chi_{i,k|k-1}^{x}$$

$$\hat{y}_k^- = \sum_{i=0}^{2L} \beta_i^{(m)} \mathcal{Y}_{i,k|k-1}$$

$$P_k^- = \sum_{i=0}^{2L} \beta_i^{(c)} \left[\chi_{i,k|k-1}^{x} - \hat{x}_k^-\right]\left[\chi_{i,k|k-1}^{x} - \hat{x}_k^-\right]^T$$

Measurement update:

$$P_{\tilde{d}_k, \tilde{d}_k} = \sum_{i=0}^{2L} \beta_i^{(c)} \left(\mathcal{D}_{i,k|k-1} - \hat{d}_k\right)\left(\mathcal{D}_{i,k|k-1} - \hat{d}_k\right)^T + R_k^e$$

$$P_{w_k, d_k} = \sum_{i=0}^{2L} \beta_i^{(c)} \left(\mathcal{W}_{i,k|k-1} - \hat{w}_k^-\right)\left(\mathcal{D}_{i,k|k-1} - \hat{d}_k\right)^T$$

$$\mathcal{K}_k = P_{w_k d_k} P_{\tilde{d}_k \tilde{d}_k}^{-1}$$

$$\hat{w}_k = \hat{w}_k^- + \mathcal{K}_k\left(d_k - \hat{d}_k\right)$$

$$P_{w_k} = P_{w_k}^- - \mathcal{K}_k P_{\tilde{d}_k, \tilde{d}_k} \mathcal{K}^T$$

where $x^{\alpha} = \begin{bmatrix} x^T & v^T & n^T \end{bmatrix}^T$, $\chi^{\alpha} = \begin{bmatrix} \left(\chi^x\right)^T & \left(\chi^v\right)^T & \left(\chi^n\right)^T \end{bmatrix}^T$, $\lambda =$ composite scaling parameter, $L =$ dimension of augmented state, $P_v =$ process noise covariance matrix, $\beta_i =$ weights as calculated in Equation (3.42).

3.5.3 Parameter estimation

Consider a nonlinear mapping

$$y_k = G\left(x_k, w\right) \tag{3.49}$$

where x_k is the input, y_k is the output, and the functional $G\left(x_k, w\right)$ is parameterized by the vector w. The error is defined as $e_k = d_k - G\left(x_k, w\right)$, d_k is the desired outputs corresponding to input x_k. In order to minimize the error, a new state-space representation is given,

$$w_{k+1} = w_k + r_k \tag{3.50}$$

$$d_k = G\left(x_k, w_k\right) + e_k \tag{3.51}$$

where w_k corresponds to a stationary process, driven by process noise r_k, and the output d_k corresponds to a nonlinear observation on w_k. The complete parameter estimation of the UKF is given in Table 3-4:

Table 3-4 The UKF parameter estimation algorithm

Initial estimates:

$$\hat{w}_0 = E[w]$$

$$P_{w_0} = E\left[(w-\hat{w}_0)(w-\hat{w}_0)^T\right]$$

Calculate the sigma points:

$$\hat{w}_k^- = \hat{w}_{k-1}$$

$$\boldsymbol{\mathcal{W}}_{k|k-1} = \left[\hat{w}_k^- \quad \hat{w}_k^- + \gamma\sqrt{P_{w_k}^-} \quad \hat{w}_k^- - \gamma\sqrt{P_{w_k}^-}\right]$$

Time update:

$$\hat{d}_k = \sum_{i=0}^{2L} \beta_i^{(m)} \boldsymbol{\mathcal{D}}_{i,k|k-1}$$

$$P_{w_k}^- = P_{w_{k-1}} + R_{k-1}^r$$

$$\textit{Option 1}\ \ \boldsymbol{\mathcal{D}}_{k|k-1} = G\left(x_k, \boldsymbol{\mathcal{W}}_{k|k-1}\right)$$

$$\textit{Option 2}\ \ \hat{d}_k = G\left(x_k, \hat{w}_k^-\right)$$

Measurement update:

$$P_{\tilde{d}_k,\tilde{d}_k} = \sum_{i=0}^{2L} \beta_i^{(c)} \left(\boldsymbol{\mathcal{D}}_{i,k|k-1} - \hat{d}_k\right)\left(\boldsymbol{\mathcal{D}}_{i,k|k-1} - \hat{d}_k\right)^T + R_k^e$$

$$P_{w_k,d_k} = \sum_{i=0}^{2L} \beta_i^{(c)} \left(\boldsymbol{\mathcal{W}}_{i,k|k-1} - \hat{w}_k^-\right)\left(\boldsymbol{\mathcal{D}}_{i,k|k-1} - \hat{d}_k\right)^T$$

$$\boldsymbol{\mathcal{K}}_k = P_{w_k d_k} P_{\tilde{d}_k \tilde{d}_k}^{-1}$$

$$\hat{w}_k = \hat{w}_k^- + \boldsymbol{\mathcal{K}}_k\left(d_k - \hat{d}_k\right)$$

where $\gamma = \sqrt{L+\lambda}$, λ is the composite scaling parameter, L is the dimension of the parameters to be estimated, R^r is the process-noise covariance, and R^e is the measurement-noise covariance.

3.5.4 DUKF estimation

During FDD implementation, the dual estimation problem which consists of simultaneously estimating the state x_k and the model parameters w from the noisy data y_k needs to be addressed. ATSEKF solves this issue through treating parameters which needs to be estimated as state parameters. The DUKF estimation solves this problem

through performing the state and parameter estimation simultaneously, given only noisy observations. At every time sample, the UKF state filter estimates the state using the current model estimate $\hat{w}_k$ while the UKF parameter filter estimates the parameters using the current state estimate $\hat{x}_k$. The estimation scheme is shown in Figure 3-5.

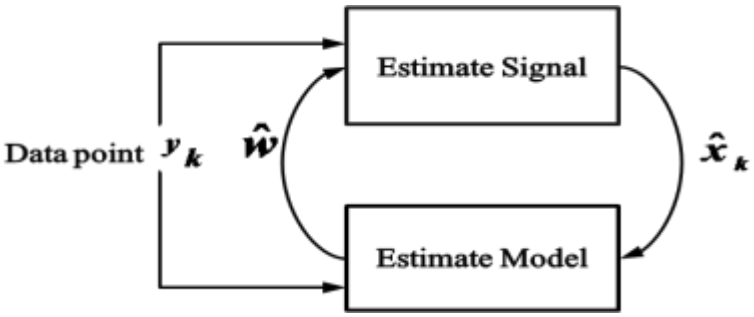

Figure 3-5 Sequential approach of DUKF designed to pass over the data one point at a time [26]

3.6 Fault detection and diagnosis decision schemes

After generation of residuals and the fault is detected by the ATSEKF and DUKF filters, the next task is to recognize and decide the best time to report the fault in a dynamic system. This step also decides the time to activate the reconfiguration module, so it should avoid to report too early or too late. This detection procedure is consisting of two steps and it is based on a statistical hypothesis test [18]. The task of the first step is to obtain the statistical quantities, such as mean values and variances, in a relatively large moving window once the system reach to steady-state condition under the normal operations. The assumption is that the residual from the state estimates and the residual from the parameter estimates follow the Normal or Gaussian distribution and are not

dependent on each other. The second phase uses a smaller moving window to determine the statistical quantities based on those from the first phase when the faults occur.

Step 1: Define $\hat{\gamma}(k) \sim \Omega\left(\bar{u}_{\gamma^0}, \sigma^2{}_{\gamma^0}\right)$, where $\hat{\gamma}(k) \in \mathbb{R}^p$ denotes the chosen residuals vector from the estimated fault parameters and the measurement residuals of the filter. $\bar{u}_{\gamma^0}$ represents the mean value of $\hat{\gamma}(k)$. $\sigma^2{}_{\gamma^0}$ denotes the associated variance.

For $i = 1, \ldots, N_1$, using

$$\bar{\mu}_{\hat{\gamma}_i^0}(k) = \frac{1}{k}\sum_{j=1}^{k} \hat{\gamma}_i(j) \tag{3.52}$$

to obtain the mean, and covariance can be obtained by

$$\sigma^2{}_{\hat{\gamma}_i^0}(k) = \frac{1}{k-1}\sum_{j=1}^{k}\left[\hat{\gamma}_i(j) - \bar{\mu}_{\hat{\gamma}_i^0}(k)\right]^2 \tag{3.53}$$

or in recursive form

$$\bar{\mu}_{\hat{\gamma}_i^0}(k) = \frac{k-1}{k}\bar{\mu}_{\hat{\gamma}_i^0}(k-1) + \hat{\gamma}_i(k) \tag{3.54}$$

$$\sigma^2{}_{\hat{\gamma}_i^0}(k) = \frac{k-2}{k-1}\sigma^2{}_{\hat{\gamma}_i^0}(k-1) + \frac{1}{k}\left[\hat{\gamma}_i(k) - \bar{\mu}_{\hat{\gamma}_i^0}(k-1)\right]^2 \tag{3.55}$$

N_1 is the sample size of a discrete random vector, and generally it is chosen to ensure a sufficient accuracy of getting the statistical quantities of the normal operations.

Step 2: Determine the statistical quantities under the abnormal operation.

Define the following calculation with moving window of size N_2 based statistical quantities

$$\bar{\mu}_{\hat{\gamma}_i}(k) = \frac{1}{N_2}\sum_{j=k-N_2+1}^{k}\hat{\gamma}_i(j)$$

$$= \bar{\mu}_{\hat{\gamma}_i}(k-1) - \frac{1}{N_2}\left[\hat{\gamma}_i(k-N_2) - \hat{\gamma}_i(k)\right]$$

$$= \bar{\mu}_{\hat{\gamma}_i}(k-1) - \frac{1}{N_2}\delta_i(k) \tag{3.56}$$

$$\sigma^2{}_{\hat{\gamma}_i^{\mathrm{I}}}(k) = \frac{1}{N_2-1}\sum_{j=k-N_2+1}^{k}\left[\hat{\gamma}_i(j) - \bar{\mu}_{\hat{\gamma}_i^0}\right]^2 \tag{3.57}$$

$$\sigma^2{}_{\hat{\gamma}_i^{\Pi}}(k) = \frac{1}{N_2-1}\sum_{j=k-N_2+1}^{k}\left[\hat{\gamma}_i(j) - \bar{\mu}_{\hat{\gamma}_i}(k)\right]^2 \tag{3.58}$$

Then, a fault in the system corresponding to the *i*th residual is declared at time *k* if the following detection variable

$$d_i(k) = \frac{\sigma^2{}_{\hat{\gamma}_i^{\mathrm{I}}}(k)}{\sigma^2{}_{\hat{\gamma}_i^0}(k)} - \ln\frac{\sigma^2{}_{\hat{\gamma}_i^{\Pi}}(k)}{\sigma^2{}_{\hat{\gamma}_i^0}(k)} - 1, \quad i = 1,\ldots,p \tag{3.59}$$

exceeds a predetermined threshold ε_i

$$d_i(k) \underset{H_{\mathrm{i}}}{\overset{H_o}{\gtrless}} \varepsilon_i \tag{3.60}$$

where $H_0 = \{\text{no fault indication in } i\text{th residual}\}$, $H_i = \{\text{fault indication in } i\text{th residual}\}$. The window length N_2 is less than N_1 and the threshold ε_i is a design variable, and the

FDD will cause jitter and false alarm if ε_i is chosen too small, on the contrary, the FDD will miss detection if the threshold ε_i is set too large. By defining a threshold variable ε_i to accentuate the deviation in the statistical quantities from their normal values, the fault can be reported and reconfiguration control part can be activated at the best time.

3.7 Summary

This chapter starts from parameter estimation discussion, and later the conventional Kalman filter is presented. After that, ATSEKF is derived based on a two-stage Kalman filter originally proposed by Keller [19]. Unscented transformation is explained in this chapter, and based on UT, UKF state estimation and parameter estimation are presented respectively. This chapter presents also the FDD decision scheme adopted by this thesis work.

4 Nonlinear Dynamics and Models of Rotary- and Fixed-wing UAVs and Boeing 747 – 100/200

UAV is an aircraft without human crew on board and it can be controlled by a pilot at a ground control station or operating autonomously with autopilot during entire flight of the vehicles. UAV's history can be traced back to 1894, and the first pilotless aircraft was built shortly after World War I. The first decade of the 21st century, countries in the world develop a variety UAVs with different purposes, and currently 32 countries in the world have developed 50 kinds of UAVs [60]. UAVs have tended to be small, which are the main beneficiaries of the development of technology. UAV is now being given a greatly expanded role in war mission.

In the aviation field, UAVs are begun to be chosen as the benchmarks to validate the various FTC schemes. The small size and affordable investment attract a lot of universities and research institutes to choose it as the test bed. Furthermore, the dynamic mathematical models of UAVs are not that complicated, so compared with fixed-wing airplanes, it will be easier to do different tests. The most attractive thing is there is no pilot on board, so it is less risky to be a test bed.

In this section, two different types of UAVs will be introduced for the purpose of investigating and evaluating FDD schemes developed in Chapter 3, one is a rotary-wing quad-rotor helicopter UAV, and the other is fixed-wing general transport UAV. Boeing 747-100/200 aircraft will be introduced as the representative for the commercial aircrafts at the end of this chapter.

4.1 Quad-rotor Helicopter UAV Model

The first aircraft considered in this thesis work is a rotary-wing quad-rotor helicopter UAV as shown in Figure 4-1. The quad-rotor helicopter has been used in several domains: safety, natural risk management, intervention in hostile sites, and environmental protection [27]. The quad-rotor is a helicopter which is able to fly indoors, and it has four lift-generating propellers driven by four motors as shown in Figure 4-2.

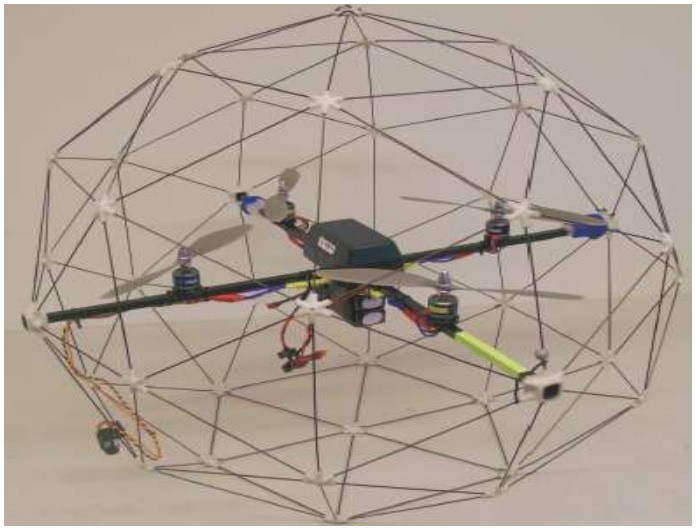

Figure 4-1 A quad-rotor helicopter

In order to balance moments and produce yaw motion, propeller pairs (1, 3) and (2, 4) respectively turn in opposite direction as shown in Figure 4-2. The front and rear motors spin their propellers clockwise to generate thrust, while the left and right motors rotate counter-clockwise. The altitude of the quad-rotor helicopter is controlled by adjusting the spinning speed of four rotors together with the same magnitude in lift forces. The yaw angle ψ is generated by creating a difference in speed between clockwise and counter-clockwise propellers. The roll angle θ depends on the 2^{nd} and 4^{th} propeller's converse

speed. The pitch angle ϕ is controlled by the 1st and 3rd propeller's converse speed. The motion in horizontal direction depends on the pitch angle and roll angle [28, 29].

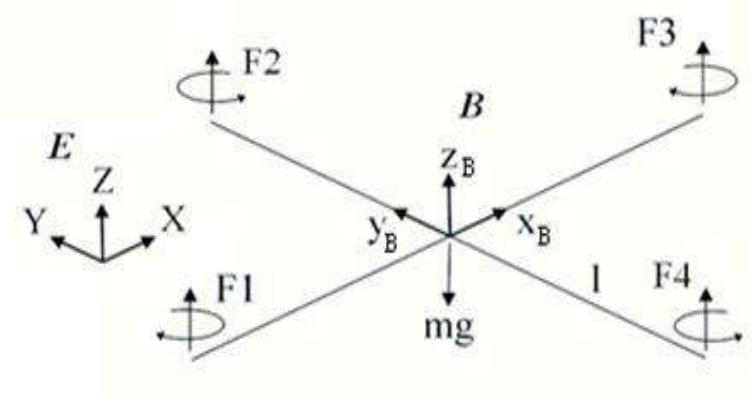

Figure 4-2 Physical structure of a quad-rotor UAV [28]

In Figure 4-2, m denotes the mass of the quad-rotor UAV, g is the gravity acceleration and $F_1, F_2, F_3,$ and F_4 denote the thrust forces which are generated by each corresponding rotor, coordinates $\{x_E, y_E, z_E\}$ represent the inertial reference frame E fixed with the earth, and coordinates $\{x_B, y_B, z_B\}$ denote the body reference frame B fixed with quad-rotor UAV body.

4.1.1 Dynamic modeling of a quad-rotor UAV

The flight dynamic equations of a quad-rotor UAV describe a rotating rigid body with six-degrees-of-freedom (6DoF). The inertial reference frame is denoted by E= {Ex,Ey,Ez}, which is fixed with the earth, and the body frame B = {Bx, By, Bz} with the quad-rotor UAV body and is assumed to be at the centre of the gravity of the quad-rotor, where the z axis is pointing upwards. The three translation components $\zeta = \begin{bmatrix} xt & yt & zt \end{bmatrix}^T$

represent the position of the quad-rotor UAV's center of mass, and three Euler's angles $\eta = [\phi \quad \theta \quad \psi]^T$ represent its orientation of a rigid body as shown in Figure 4-2, ϕ is pitch angle $\left(-\frac{1}{2}\pi < \phi < \frac{1}{2}\pi\right)$, θ is roll angle $\left(-\frac{1}{2}\pi < \theta < \frac{1}{2}\pi\right)$ and ψ is yaw angle $\left(-\frac{1}{2}\pi < \psi < \frac{1}{2}\pi\right)$, $V = [V_x \quad V_y \quad V_z]^T$ represents three translation velocities, and $\Omega = [\Omega_\phi \quad \Omega_\theta \quad \Omega_\psi]^T$ represents three rotation velocities.

The dynamic model is derived using Euler-Lagrange formalism [4] under the following assumptions:

- The structure is supposed to be rigid.
- The structure is supposed to be symmetrical.
- The center of mass and the body fixed frame origin are assumed to coincide.
- The propellers are supposed rigid.
- The thrust and drag are proportional to the square of the propeller speed.

The relation between ζ, η and V, Ω is

$$\begin{aligned} \dot{\zeta} &= R_t V \\ \Omega &= R_r \dot{\eta} \end{aligned} \tag{4.1}$$

R_t and R_r are the transformation velocity matrix and the rotation velocity matrix.

$$R_t = \begin{bmatrix} \cos\phi\cos\psi & \sin\phi\sin\theta\cos\psi - \cos\phi\sin\psi & \cos\phi\sin\theta\cos\psi + \sin\phi\sin\psi \\ \cos\theta\sin\psi & \sin\phi\sin\theta\sin\psi + \cos\phi\cos\psi & \cos\phi\sin\theta\sin\psi - \sin\phi\cos\psi \\ -\sin\phi & \sin\phi\cos\theta & \cos\phi\cos\theta \end{bmatrix} \tag{4.2}$$

$$R_r = \begin{bmatrix} 1 & 0 & -\sin\theta \\ 0 & \cos\phi & \cos\theta\sin\phi \\ 0 & -\sin\phi & \cos\phi\cos\theta \end{bmatrix} \tag{4.3}$$

$$\dot{R}_t = R_t \times \begin{bmatrix} 0 & -\Omega_3 & \Omega_2 \\ \Omega_3 & 0 & -\Omega_1 \\ -\Omega_2 & \Omega_1 & 0 \end{bmatrix} \tag{4.4}$$

The derivative of Equation (4.1) with respect to time is given as:

$$\begin{aligned} \ddot{\zeta} &= R_t\dot{V} + \dot{R}_t V = R_t\left(\dot{V} + \Omega \times V\right) \\ \dot{\Omega} &= R_r\ddot{\eta} + \left(\frac{\partial R_t}{\partial \phi}\dot{\phi} + \frac{\partial R_r}{\partial \theta}\dot{\theta}\right)\dot{\eta} \end{aligned} \tag{4.5}$$

Using the Newton's 2nd laws in the reference frame E^m, external vertical forces F_{total} and moments T_{total} can be represented as:

$$\begin{aligned} F_{total} &= m\dot{V} + \Omega \times (mV) \\ T_{total} &= I\dot{\Omega} + \Omega \times (I\Omega) \end{aligned} \tag{4.6}$$

where m is the mass of the quad-rotor UAV and I is the total inertia matrix of the quad-rotor UAV, $I = diag\left[I_u, I_v, I_w\right]$, I_u, I_v and I_w are moments of inertia in the body reference frame.

$$
\begin{aligned}
F_e &= F + F_a + F_g = \begin{bmatrix} 0 \\ 0 \\ c_t \sum_{i=1}^{4} \omega_i^2 \end{bmatrix} - K_t V - m \begin{bmatrix} -\sin\theta \\ \sin\phi\cos\theta \\ \cos\phi\cos\theta \end{bmatrix} g \\
T_e &= T + T_a + T_g = \begin{bmatrix} dc_t\left(\omega_2^2 - \omega_4^2\right) \\ dc_t\left(\omega_3^2 - \omega_1^2\right) \\ c_d \sum_{i=1}^{4} (-1)^{i+1} \omega_i^2 \end{bmatrix} - K_r \Omega - \sum_{i=1}^{4} \Omega \times I_R W_i
\end{aligned}
\tag{4.7}
$$

$$
\begin{aligned}
\ddot{x} &= \frac{F_1 + F_2 + F_3 + F_4}{m}\left(\cos\psi\sin\theta\cos\phi + \sin\psi\sin\phi\right) - \frac{k_{d1}\dot{x}}{m} \\
\ddot{y} &= \frac{F_1 + F_2 + F_3 + F_4}{m}\left(\sin\psi\sin\theta\cos\phi - \cos\psi\sin\phi\right) - \frac{k_{d2}\dot{y}}{m} \\
\ddot{z} &= \frac{F_1 + F_2 + F_3 + F_4}{m}\cos\theta\cos\phi - \frac{k_{d3}\dot{z}}{m} - g \\
\ddot{\phi} &= \frac{1}{I_x}\left[\left(F_2 - F_4\right)l - k_{d4}\dot{\phi} - \dot{\theta}\dot{\psi}\left(I_z - I_y\right)\right] \\
\ddot{\theta} &= \frac{1}{I_y}\left[\left(F_1 - F_3\right)l - k_{d5}\dot{\theta} - \dot{\phi}\dot{\psi}\left(I_x - I_z\right)\right] \\
\ddot{\psi} &= \frac{1}{I_z}\left[\left(F_1 - F_2 + F_3 - F_4\right)l - k_{d6}\dot{\psi} - \dot{\theta}\dot{\phi}\left(I_y - I_x\right)\right]
\end{aligned}
\tag{4.8}
$$

where force F_{total} is the total force acting on the quad-rotor UAV's center of gravity, force F is generated by four rotors, force F_a is considered as a disturbance, and force F_g is the gravity. T_{total} is the total torque acting on the quad-rotor UAV's center of gravity, the torque T is generated by rotors, the aerodynamic torque T_a is considered as a disturbance and the torque T_g is created by gravity. $\{K_t, K_r\}$ are two diagonal aerodynamic matrices, $W_i = \left[0, 0, (-1)^{i+1}\omega_i\right]^T$ is the rotational velocity vector of the *i*-th rotor, and I_R is the inertia of the rotor. dc_t is the rotor distance to center of gravity along the x or y axis, c_d

is the torque/force ratio. Therefore the dynamics of rotation of the quad-rotor UAV can be expressed as:

$$\begin{aligned} F &= mR_t^T \ddot{\zeta} + K_t R_t^T \dot{\zeta} + m \begin{bmatrix} -\sin\theta \\ \sin\phi\cos\theta \\ \cos\phi\cos\theta \end{bmatrix} g \\ T &= IR_r\ddot{\eta} + I\left(\frac{\partial R_t}{\partial \phi}\dot{\phi} + \frac{\partial R_r}{\partial \theta}\dot{\theta}\right)\dot{\eta} + K_r R_r \dot{\eta} + \left(R_r\dot{\eta}\right)\times\left(IR_r\dot{\eta} + \sum_{i=1}^{4} I_R W_i\right) \end{aligned} \tag{4.9}$$

Therefore, the position (x, y) are controlled by a virtual input based on the tilt angles (ϕ, θ), and the (ϕ, θ) and the (ψ, z) motions are controlled by $\omega_i, i = 1, \cdots, 4$. The quad-rotor is driven by four DC motors:

$$\begin{aligned} L\frac{di}{dt} &= u - \Re i - k_e \omega \\ I_R\frac{d\omega}{dt} &= k_m i - k_r \omega^2 - k_s \end{aligned} \tag{4.10}$$

where u is the controllable input, i is the electrical current of motors, $\Re$ is the electrical resistance and ω is the rotation speed of rotor.

4.2 The NASA GTM Fixed-wing UAV Model

In order to investigate flight dynamics and study the behavior of the aircraft in upset conditions, NASA built a test bed referred as to the Generic Transport Model (GTM) that can fly outdoors. The GTM is a 6 degree-of-freedom (DOF) nonlinear model with 5.5% dynamically scaled, turbine powered fixed-wing unmanned aerial vehicle [30] as shown in Figure 4-3. The simulation environment is implemented by the Matlab/Simulink, while the two physical UAVs are available at a NASA research center for experimental tests.

This thesis focuses on developing FDD schemes based on a Linear Parameter Varying (LPV) model [31] of the GTM and a high fidelity nonlinear model of the GTM in the event of actuator faults or failures. The FDD scheme utilizes ATSEKF and DUKF with real time states estimation and fault parameters identification based on the measured outputs of the sensors and the inputs to the actuators under the high fidelity 6 DOF nonlinear Matlab/Simulink environment.

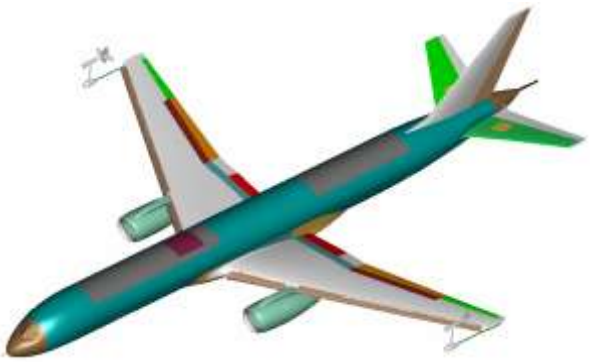

Figure 4-3 The NASA generic transport model (GTM)

4.2.1 Nonlinear model of the GTM

The state variables of the aircraft is defined as $x = \begin{bmatrix} u & v & w & p & q & r & \phi & \theta & \psi \end{bmatrix}^T$. u is velocity along *x*-axis with body frame, v is velocity along *y*-axis with body frame, w is velocity along *z*-axis with body frame, p is roll angular rate, q is pitch angular rate, r is yaw angular rate, ϕ is roll angle fixed with Earth frame, θ is pitch angle fixed with Earth frame and ψ is yaw angle fixed with Earth frame.

In order to simply the dynamic equations, following assumptions are made:

1) $I_{xy} = 0$ and $I_{yz} = 0$;

2) Mass is assumed to remain constant;

3) The center of gravity is assumed to be constant and fixed at the nominal value.

Nonlinear dynamic equations of the GTM are represented as:

$$\dot{u} = \left[C_{\alpha,\beta} + C_{X_{\hat{q}}} + C_{X_{\delta_e}} + C_{X_{\delta_T}} + \left(C_{X_{\delta_R}} + C_{X_{\delta_\alpha}} \right) \right] \frac{S\bar{q}}{m} - g\sin\theta + rv - qw \tag{4.11}$$

$$\dot{w} = \left[C_{Z_{\alpha,\beta}} + C_{Z_{\hat{q}}} + C_{Z_{\delta_e}} + C_{Z_{\delta_T}} + \left(C_{Z_{\delta_T}} + C_{Z_{\delta_\alpha}} \right) \right] \frac{S\bar{q}}{m} + g\cos\theta\sin\phi - ru + pw \tag{4.12}$$

$$\dot{q} = \left[C_{m_{\alpha,\beta}} + C_{m_{\hat{q}}} + C_{m_{\delta_e}} + C_{m_{\delta_T}} + \left(C_{m_{\delta_R}} + C_{m_{\delta_\alpha}} \right) \right] S\bar{q}c \frac{1}{I_{yy}} + rp\left(I_{zz} - I_{yy} \right) + I_{xz}\left(p^2 - r^2 \right) \frac{1}{I_{yy}} \tag{4.13}$$

$$\dot{v} = \left[C_{Y_{\alpha,\beta}} + C_{Y_{\hat{p}}} + C_{Y_{\delta_R}} + C_{Y_{\delta_\alpha}} + \left(C_{Y_{\delta_e}} + C_{Y_{\hat{r}}} \right) \right] \frac{S\bar{q}}{m} + g\cos\theta\cos\phi + qu - pv \tag{4.14}$$

$$D = \left[C_{l_{\alpha,\beta}} + C_{l_{\hat{p}}} + C_{l_{\delta_R}} + C_{l_{\delta_\alpha}} + \left(C_{l_{\delta_e}} + C_{l_{\hat{r}}} \right) \right] S\bar{q}b + rp\left(I_{zz} - I_{yy} \right) + I_{xz} \tag{4.15}$$

$$E = \left[C_{m_{\alpha,\beta}} + C_{m_{\hat{p}}} + C_{m_{\delta_R}} + C_{m_{\delta_\alpha}} + \left(C_{m_{\delta_e}} + C_{m_{\hat{r}}} \right) \right] S\bar{q}b + pq\left(I_{yy} - I_{xx} \right) + I_{xz} \tag{4.16}$$

$$\dot{p} = \frac{I_{yy}I_{zz}D + I_{xz}I_{yy}E}{I_{yy}I_{xx} + {I_{xz}}^2 I_{yy}} \tag{4.17}$$

$$\dot{r} = \frac{I_{yy}I_{xz}D + I_{xx}I_{yy}E}{I_{yy}I_{xx} + {I_{xz}}^2 I_{yy}} \tag{4.18}$$

$$\dot{\phi} = p + \frac{\sin\phi\sin\theta q + \cos\phi\sin\theta r}{\cos\theta} \tag{4.19}$$

$$\dot{\theta} = \cos\phi q - \sin\phi r \tag{4.20}$$

$$\dot{\psi} = \frac{\sin\phi q + \cos\phi r}{\cos\theta} \tag{4.21}$$

The lift, drag and pitching moment coefficients are implemented by lookup tables in the Matlab/Simulink simulation environment.

4.2.2 Linear parameter varying (LPV) model of the GTM

As the emerging approach to control theory, Linear Parameter Varying (LPV) modeling and control of nonlinear systems have been widely studied in dynamic systems since early 1990s [31, 34]. Applications have been successful in some levels. An LPV model simulates the actual nonlinear system by using time-varying real parameters like altitude and/or speed to obtain smooth semi-linear models. However, there is a few of investigations for FDD design with LPV model, except the work presented in [35]. Since FDD in this thesis work is a model-based estimation, the LPV model is chosen for the FDD design to the nonlinear model of the GTM due to real-time implementation consideration. This thesis work presents implementation of the ATSEKF and DUKF schemes in the GTM LPV model.

For the sake of brevity, the basic definition of an LPV model for a nonlinear system is presented. LPV model is a class of finite dimensional linear models of a nonlinear system whose state-space entries *A*, *B*, *C*, and *D* depend continuously on a time-varying parameter vector, $\rho(t)$ [36]. Parameters $\rho(t)$ can be measured at the current time and their values are constrained *a priori* to lie in some known, bounded set and this set is continuous, but cannot be known in advance. The formal definition of an LPV model can be given as follows [57]:

Given a compact subset $\mathcal{P} \subset \Re^s$, the parameter variation set $\mathcal{F}_\mathcal{P}$ denotes the set of all piecewise continuous functions mapping $\Re^+$ (time) into ρ with a finite number of discontinuities in any interval.

Given continuous functions: $A: \Re^s \to \Re^{n \times n}$, $B: \Re^s \to \Re^{n \times n_u}$, $C: \Re^s \to \Re^{n_y \times n}$ and $D: \Re^s \to \Re^{n_y \times n_u}$, an *n*-th order linear parameter-varying (LPV) model of a given nonlinear system is defined as:

$$\begin{bmatrix} \dot{x}(t) \\ y(t) \end{bmatrix} = \begin{bmatrix} A(\rho(t)) & B(\rho(t)) \\ C(\rho(t)) & D(\rho(t)) \end{bmatrix} \begin{bmatrix} x(t) \\ u(t) \end{bmatrix} \tag{4.22}$$

where $\rho \in \mathcal{F}_\mathcal{P}$.

Now the key task is to select an adequate $\rho(t)$ such that the above LPV model is able to capture the nonlinearities of the system. So far, there are three techniques for obtaining LPV models from a nonlinear system [33].

1) **Jacobian linearization approach**. It is implemented at a number of selected equilibrium points. The Jacobian linearization approach uses first-order Taylor series expansion of nonlinear model to create an LPV model which approximates the nonlinear system with respect to selected equilibrium points. The drawback of this approach is that it is easy to divergent and hard to obtain the transient behavior of the nonlinear system.
2) **State transformation approach**. This approach is proposed based on exact state transformations at a number of selected equilibrium points. It requires that $\rho(t)$

must be available in real-time for measurement. The disadvantage of this approach is that the existence of trim map for the entire flight envelope of interest for a particular combination of the scheduling variables is not guaranteed [36].

3) **The function substitution approach**. This approach is to obtain a LPV model at a unique trim point by decomposing the nonlinear function. The main drawback of this approach is the lack of theoretical validation.

The nonlinear equations for the longitudinal motion of the GTM given as follows [33] were derived based on the Jacobian linearization approach:

$$V_{EAS} = \frac{1}{m}\left(F_x \cos\alpha + F_z \sin\alpha\right) \tag{4.23}$$

$$\dot{\alpha} = \frac{1}{mV_{EAS}}\left(-F_x \sin\alpha + F_z \cos\alpha\right) + q \tag{4.24}$$

$$\dot{\theta} = q \tag{4.25}$$

$$\dot{q} = \frac{M_y}{I_{yy}} \tag{4.26}$$

These equations contain transcendental functions and aerodynamic data obtained through wind tunnel tests and flight tests. The transcendental functions can be approximated by third-order Taylor series expansion as follows:

$$\sin\left(x\right) = x - \frac{1}{6}x^3 \tag{4.27}$$

$$\cos x = 1 - \frac{1}{2}x^2 \tag{4.28}$$

The aerodynamic data which are obtained by using lookup tables in the nonlinear model of the GTM can be approximated by polynomial equations [35]. The LPV model of the longitudinal motion of the GTM has state variables $x = \begin{bmatrix} V_{EAS} & \alpha & q & \theta \end{bmatrix}^T$, with equivalent airspeed (V_{EAS}), pitch angle rate (q), angle of attack (α), and pitch angle (θ). The input vector, *u*, is given by $u = \begin{bmatrix} \delta_{ele} & \delta_{throttle} \end{bmatrix}^T$, with δ_{ele} representing elevator deflection and $\delta_{throttle}$ representing throttle deflection. Therefore aerodynamic forces F_x and F_z and moment M_y are obtained through the following equations:

$$F_x = \bar{q} S_{ref} \left[C_x(\alpha) + C_x(\alpha, \delta_e) + C_x(\alpha, \hat{q}) \right] + 2T_X(\delta_{th}) - mg \sin\theta \tag{4.29}$$

$$F_z = \bar{q} S_{ref} \left[C_z(\alpha) + C_z(\alpha, \delta_e) + C_z(\alpha, \hat{q}) \right] + 2T_Z(\delta_{th}) + mg \cos\theta \tag{4.30}$$

$$M_y = \bar{q} S_{ref} \bar{c} \left[C_m(\alpha) + C_m(\alpha, \delta_e) + C_m(\alpha, \hat{q}) \right] + 2\Delta Z_{ENG} T_X(\delta_{th}) \tag{4.31}$$

where the aerodynamic coefficients of angle of attack α, pitch rate q and elevator deflection δ_e are obtained through lookup tables.

In the original LPV model of the GTM, fault models were not included. Partial loss of control effectiveness in elevator has been implemented for FDD purpose in this work.

4.3 Boeing 747-100/200 Aircraft Model

The third aircraft model used in this thesis is a Boeing 747 series 100/200 airplane model. The Boeing 747 (as shown in Figure 4-4) is a large, international wide-body (two-aisle) airliner with four fan jet engines designed to operate in international airports. For

Boeing 747, the longitudinal control is performed through a movable horizontal stabilizer with four elevator segments (inboard and outboard elevators) and the engine thrust. Under normal operation, the inboard and outboard elevators move together. The polynomial function model of the longitudinal motion of Boeing 747-100/200 aircraft is developed in [36]. The aerodynamic coefficients are fitted as polynomial functions of angle of attack and velocity over the given flight envelope.

4.3.1 Nonlinear model of the Boeing 747

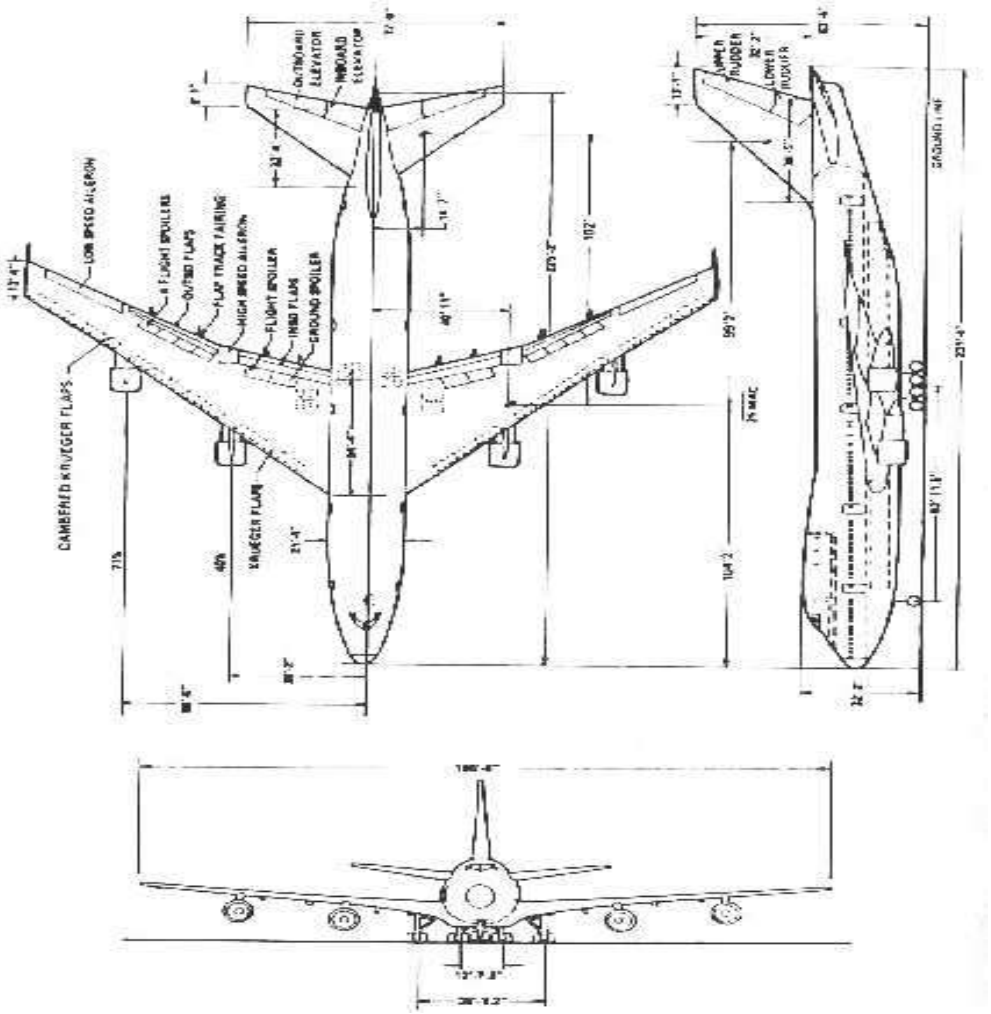

Figure 4-4 Boeing 747

The nonlinear equations of the Boeing 747 longitudinal motion are taken from [36]. The longitudinal motion of an aircraft can be defined by the following six variables: angle of attack, α, pitch rate, q, pitch angle, θ, true airspeed, V_{TAS}, altitude, h_e, and distance along the *x*-axis path x_e (recall $e \equiv$ Earth-reference-frame).

The detailed body-axes nonlinear equations for the longitudinal motion of the Boeing 747 are presented as follows [36]:

$$\dot{\alpha} = \left[1 - \frac{\bar{q}S\bar{c}}{2mV^2}\left(1.45 - 1.8x_{cg}\right)\frac{dC_L}{dq}\right]q + \left[-\frac{\bar{q}S}{mV}K_\alpha \frac{dC_L}{d\delta_e}\right]\delta_e + \left[-\frac{4}{mV}\left(\sin\alpha + 0.0436\cos\alpha\right)\right]T + \frac{1}{V}\left(\sin\alpha\sin\theta + \cos\alpha\cos\theta\right)g - \frac{\bar{q}S}{mV}C_{Lbasic} \tag{4.32}$$

$$\dot{q} = \frac{c_7\bar{q}S\bar{c}^2}{2V}\left[\frac{dC_m}{dq} - \frac{1}{\bar{c}}\left(1.45 - 1.8x_{c.g.}\right)\frac{dC_L}{dq}\left(\cos\alpha\bar{x}_{c.g.} + \sin\alpha\bar{z}_{c.g.}\right)\right]q + c_7\bar{q}S\bar{c}K_\alpha\left[\frac{dC_m}{d\delta_e} - \frac{1}{\bar{c}}\frac{dC_L}{d\delta_e}\left(\cos\alpha\bar{c}_{c.g.} + \sin\alpha\bar{z}_{c.g.}\right)\right]\delta_e + c_7\bar{q}S\bar{c}K_\alpha\frac{dC_m}{d\delta_e}\delta_s + c_7S_{zeng}T + c_7\bar{q}S\bar{c}C_{mbasic} + c_7\bar{q}S\left[C_{DMach}\left(\cos\alpha\bar{z}_{c.g.} - \sin\alpha\bar{x}_{c.g.}\right) - C_{Lbasic}\left(\cos\alpha\bar{x}_{c.g.} + \sin\alpha\bar{z}_{c.g.}\right)\right] \tag{4.33}$$

$$\dot{V} = \frac{4}{m}\left(\cos\alpha - 0.0436\sin\alpha\right)T + \left(\sin\alpha\cos\theta - \cos\alpha\sin\theta\right)g - \frac{\bar{q}S}{m}C_{CMach} \tag{4.34}$$

$$\dot{\theta} = q \tag{4.35}$$

$$\dot{h}_e = \left(\cos\alpha\sin\theta - \sin\alpha\cos\theta\right)V \tag{4.36}$$

It can also be rewritten in following matrix form:

$$\begin{bmatrix} \dot{\alpha} \\ \dot{V} \\ \dot{q} \\ \dot{\theta} \\ \dot{h}_e \end{bmatrix} = A(\alpha, V, \theta, h_e) \begin{bmatrix} \alpha \\ V \\ q \\ \theta \\ h_e \end{bmatrix} + B(\alpha, V, h_e) \begin{bmatrix} \delta_e \\ \delta_s \\ T \end{bmatrix} + f(\alpha, V, \theta, h_e, q) \tag{4.37}$$

There are three simplified inputs: elevator deflection δ_e, stabilizer deflection δ_s and engine thrust T. Altitude h_e is around 7000 m, angle of attack $\alpha \in [-2,10]$ and total airspeed $V \in [150, 280]$. In longitudinal motion, the sideslip angle, β, roll angle, ϕ, roll rate, p, and yaw rate, r, are considered to be zero.

4.4 Summary

This chapter derives the dynamic mathematical model of a quad-rotor helicopter UAV, and explains the simulation structure of the quad-rotor UAV. The nonlinear model and LPV model of the NASA's GTM is then presented in this chapter. Simulation structure of the GTM is also presented. The nonlinear dynamic model of Boeing 747 is further presented as the third benchmark model for FDD investigation.

5 Simulation Results and Analyses

The ATSEKF and DUKF have been tested on the quad-rotor UAV, Boeing 747 and GTM models. This chapter will present the simulation and analysis results respectively.

5.1 Application to Quad-rotor UAV

The system state and observation equations are modeled in discrete-time domain with Gaussian white noise. Although this is a time-variant system model, which means that the trim point, output bias and the parameters are dynamic and could be functions of time and the current state of aerial vehicle. In order to simplify the implementation of FDD, only an equilibrium point was considered in this thesis.

The linear quad-rotor UAV FDD simulation starts from the initial value $X=\begin{bmatrix}0 & 0 & 0 & 0 & 0 & 0 & 0 & 0 & 0 & 1 & 1 & 0\end{bmatrix}^T$. The measurement time interval is T=0.01s, and the UKF parameters are listed below:

$$\begin{cases}\alpha=1\\ \beta=2\\ k=3-L, L=30\\ Pw=0.001*I_{4\times4}\\ Rr_{ukfpe}=diag\left((1/0.99985-1)\right)*Pw\\ \mathrm{Re}_{ufkpe}=0.009^2*I_{6\times6}\\ Rn=I_{6\times6}\\ Px=I_{12\times12}\end{cases}.$$

The measured outputs and control signals are used as inputs for the ATSEKF and DUKF. The estimated states $\hat{x}$ and the estimated parameters are used for comparison and decision making in the detection and diagnosis logic block.

5.1.1 Application with a Linear Quad-rotor UAV Model

The ATSEKF and DUKF are implemented with the linearized quad-rotor UAV model. Simulation results under different levels of partial loss of different actuators are given below. The scenario is that the 1st propeller effectiveness encounters a 30% partial loss at time of 60 seconds.

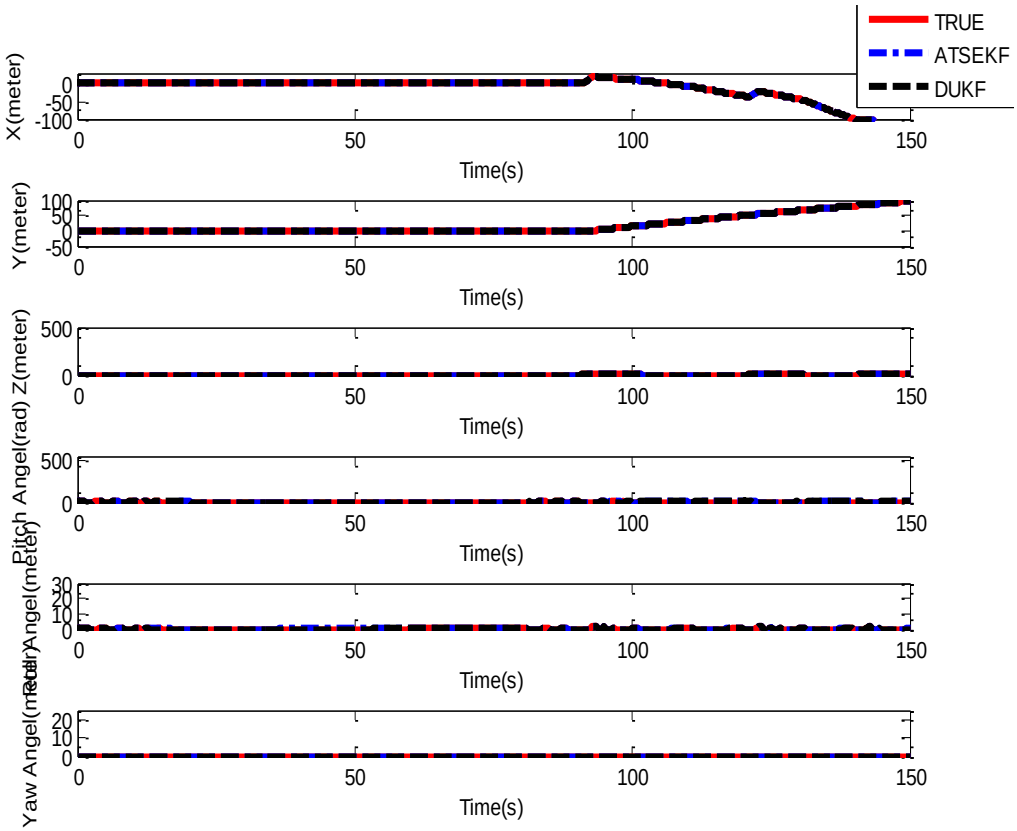

Figure 5-1 State estimation $(X, Y, Z, \phi, \theta, \psi)$

In Figure 5-1, the red solid line represents the system real outputs, the blue dash-dot line represents the state estimation outputs of ATSEKF and the black dash line represents the state estimation outputs of DUKF. The state estimation results shows that the state estimation results of ATSEKF and DUKF match the system measurement outputs well with linearized model.

Figure 5-2 below presents the fault detection residual of each propeller when partial loss occurs on the 1st propeller, and the results are obtained through Equation (3.60). Obviously, the results of ATSEKF and DUKF are not satisfactory. Since four propellers couple closely, and when the 1st propeller encounters partial loss, the rest of propellers are affected.

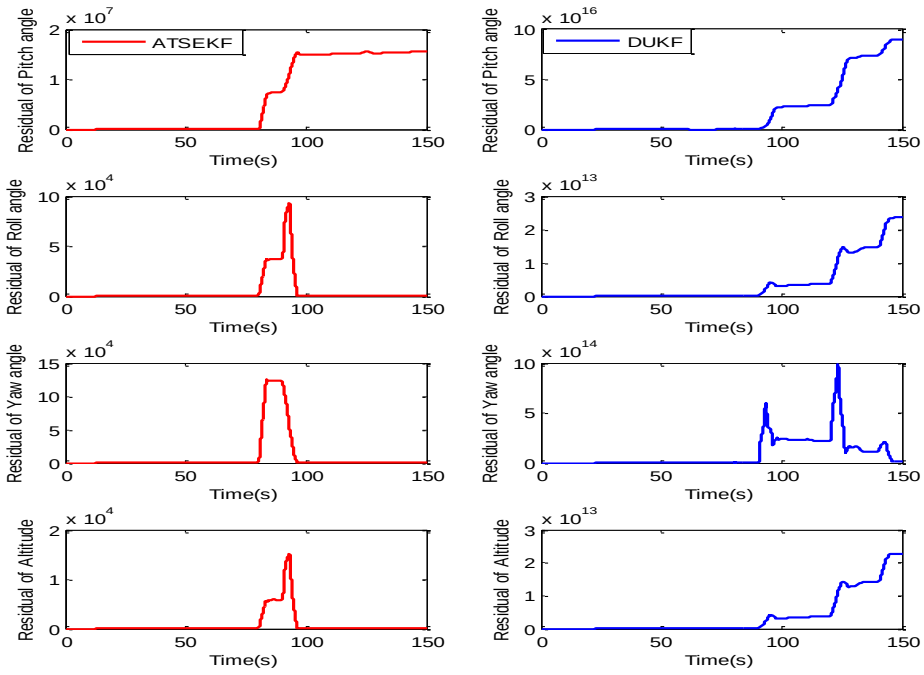

Figure 5-2 Residual of each propeller's control effectiveness

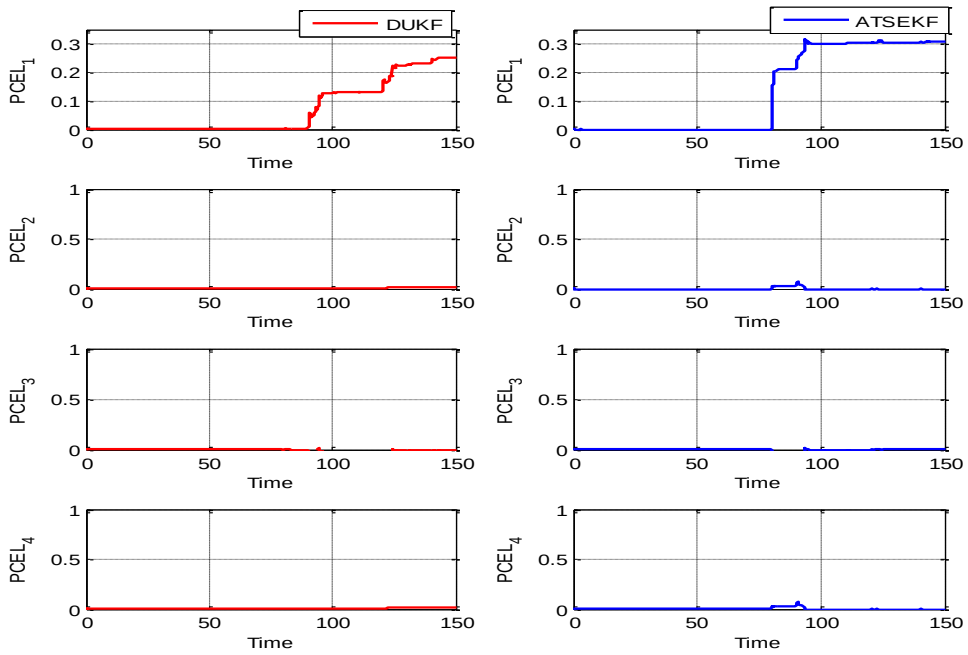

Figure 5-3 Propeller's control effectiveness estimation (1st propeller encounters a 30% partial loss at the time of 60 seconds)

On Figure 5-3, the left column plots show the four propellers' control effectiveness estimation results by DUKF, while the right column plots are the control effectiveness estimation results by ATSEKF. The parameter estimation results show that both DUKF and ATSEKF can detect the partial loss with a certain delay, but only ATSEKF can provide good estimation of the magnitude of the fault.

From Figure 5-1 to Figure 5-3, the simulation results show that both the ATSEKF and DUKF have the same performance on states estimation, the ATSEKF has better performance than the DUKF in terms of fault diagnosis in this quad-rotor UAV application, since the DUKF is more influenced by the coupled four propellers of the quad-rotor UAV than the ATSEKF with the linearized environment.

5.1.2 Application with a nonlinear quad-rotor UAV model

The ATSEKF and DUKF are implemented with the nonlinear quad-rotor UAV model in this case. The scenario is that the 1st propeller's control effectiveness encounters a 30% partial loss at time of 60 sec.

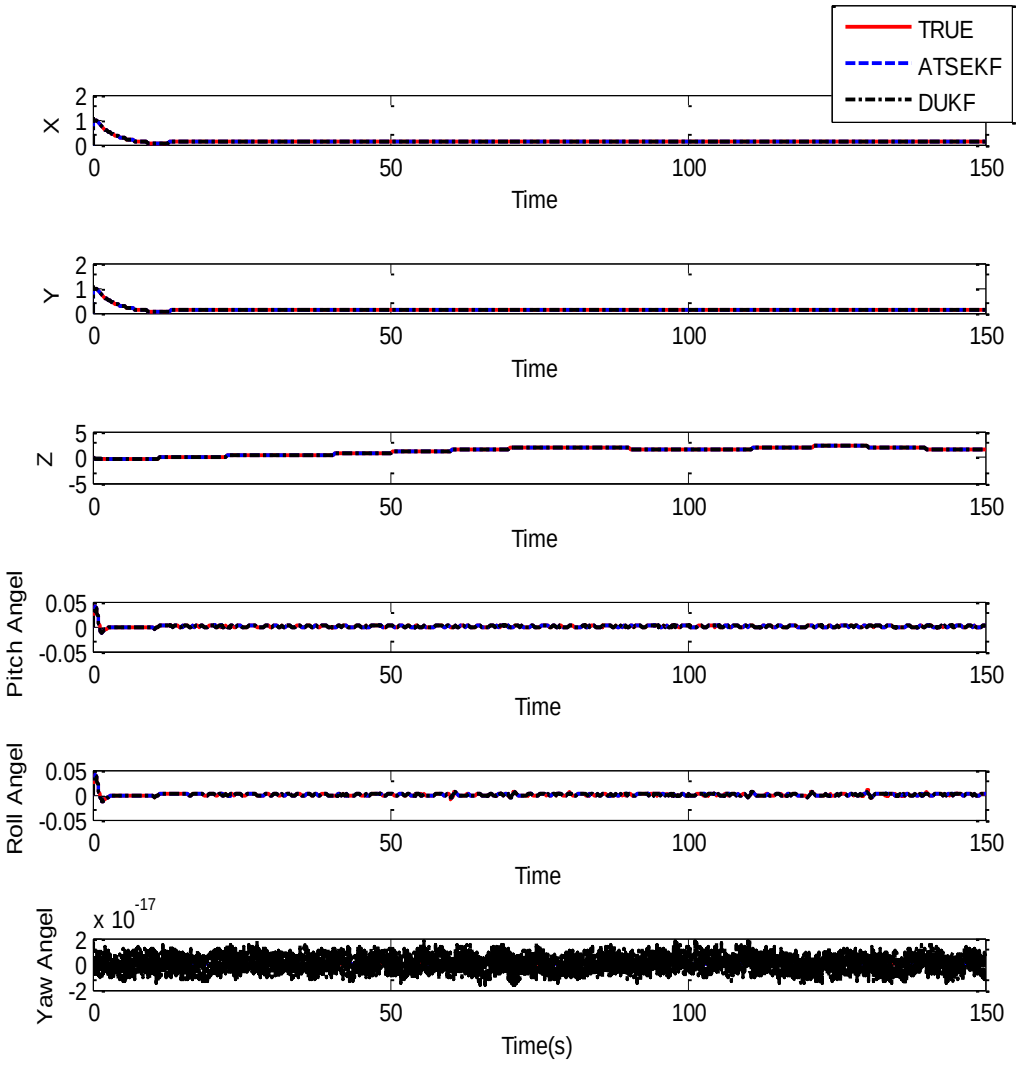

Figure 5-4 State estimation $(X, Y, Z, \phi, \theta, \psi)$

In Figure 5-4, the red solid line represents the system real outputs, the blue dash-dor line represents the state estimation outputs of ATSEKF and the black dash line represents the state estimation outputs of DUKF. The state estimation results show that the state estimation results of ATSEKF and DUKF with nonlinear model match the system measurement outputs well.

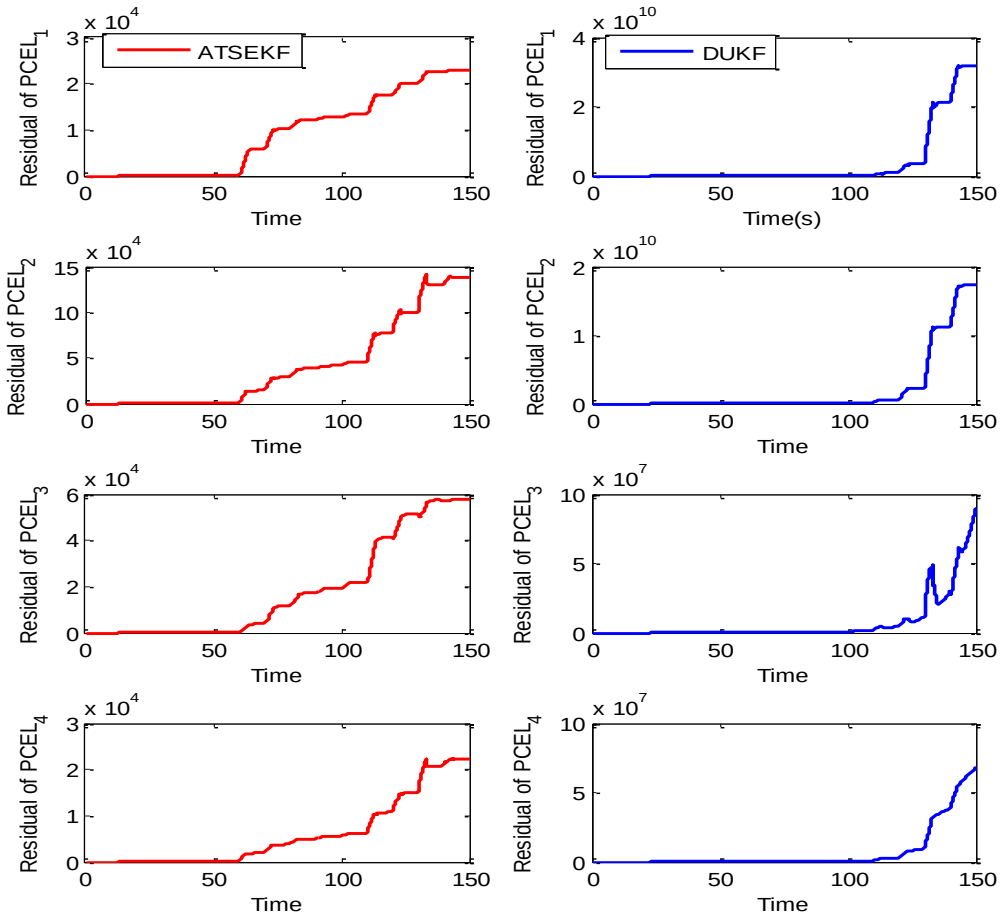

Figure 5-5 Residual of propeller's control effectiveness

Figure 5-5 is the residual of each propeller when partial loss occurs on the 1st propeller, and the results are obtained through Equation (3.60). The results of ATSEKF and DUKF

are not satisfactory, since the quad-rotor UAV is high nonlinear system and four propellers couple closely, and therefore as 1st propeller encounters partial loss, the rest of propellers are affected.

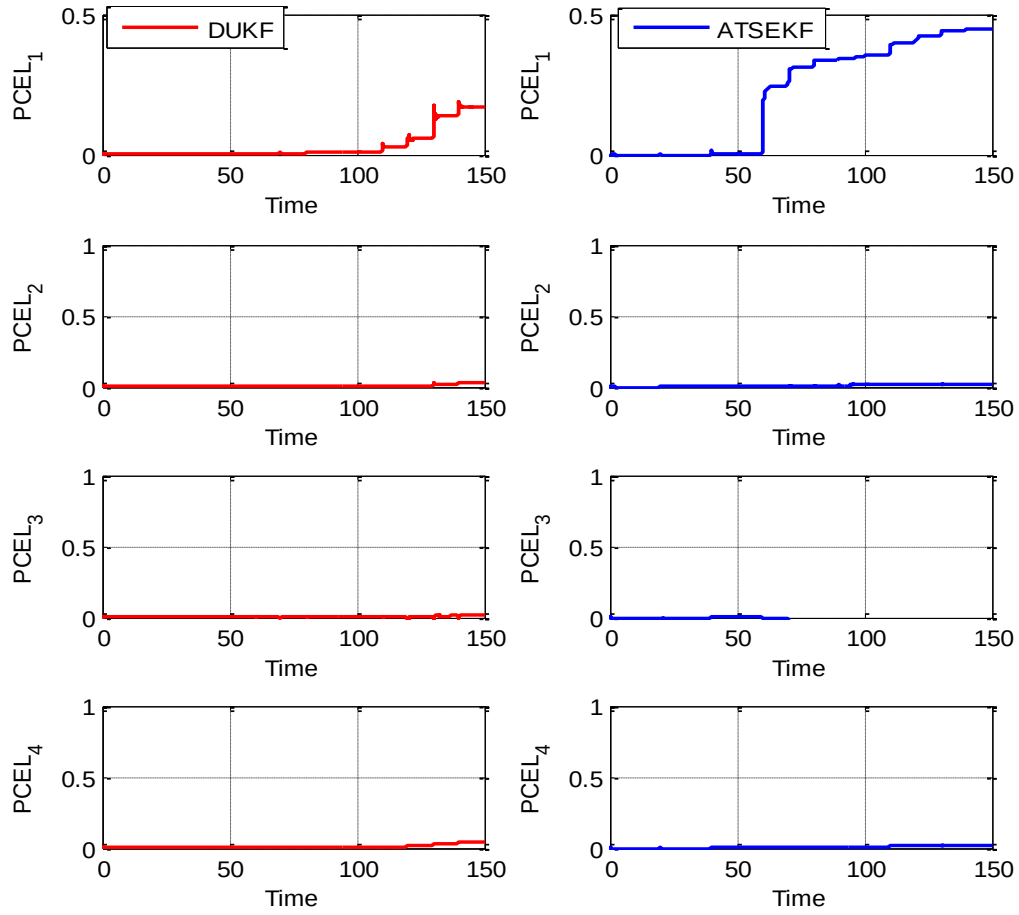

Figure 5-6 Propeller's control effectiveness estimation (1st propeller encounters a 30% partial loss at the time of 60 seconds)

On Figure 5-6, the left column plots show the four propellers' control effectiveness estimation results with DUKF, while the right column plots are the control effectiveness estimation results with ATSEKF. The parameter estimation results show that both DUKF

and ATSEKF can detect the partial loss with a certain delay, but both of them cannot provide good estimation of the magnitude of the fault.

From the results presented in Figure 5-4 to Figure 5-6, it can be easily seen that the estimated states of the ATSEKF and DUKF matched well with the measured outputs and also it filtered the measurement noise. Because the four propellers of the quad-rotor model are coupled closely, it can be seen that when one parameter changes greatly, it causes the other three parameters to change accordingly. It can be seen that the result of fault isolation is not satisfactory, and still the ATSEFK has the better performance in terms of fault diagnosis.

For the parameter estimation of the quad-rotor UAV with the linear model, the simulation results have indicated no difference between the performance of ATSEKF and DUKF. Both of them matched well with the measured outputs and also the measurement noise was fairly well filtered. However, the parameter estimates from the ATSEKF and DUKF showed that these two Kalman filters did not provide accurate estimation of the magnitude of the fault parameter, but still indicated the time when the faults occurred.

5.2 Application to the NASA's GTM UAV

In this section, simulation results and analyses of nonlinear GTM model and LPV model of the GTM are presented. In this thesis, it is assumed that failure occurs in the elevator actuator while others remain healthy. The throttle is kept constant at its trim setting throughout the maneuver.

5.2.1 Application with a nonlinear GTM UAV model

In the nonlinear model of the GTM, the scenario is that a 20% of loss of control effectiveness fault in elevator occurred at 6 sec. The experiment starts with the initial states: $X = [153.1694729 \quad 7.847030096 \quad 0.000195679 \quad 0.051182864]^T$. Since the computation is larger, the measurement time interval in nonlinear model is $T = 0.02s$.

The UKF parameters are listed as follows:

$$\begin{cases} \alpha = 1 \\ \beta = 2 \\ k = 3 - L,\ L = 15 \\ Pw = 0.001 I_{1\times 1} \\ Rr_{ukfpe} = diag\left((1/0.99985 - 1)\right) * Pw \\ \mathrm{Re}_{ukfpe} = 0.001^2 I_{9\times 9} \\ Rv = 0.01^2 I_{9\times 9} \\ Px = I_{9\times 9} \end{cases}.$$

The measured outputs and control signals are used as inputs for the DUKF. The scenario is that the elevator control effectiveness encounters a partial loss of 20% (i.e. 80% of the original value) occurred at 6 seconds.

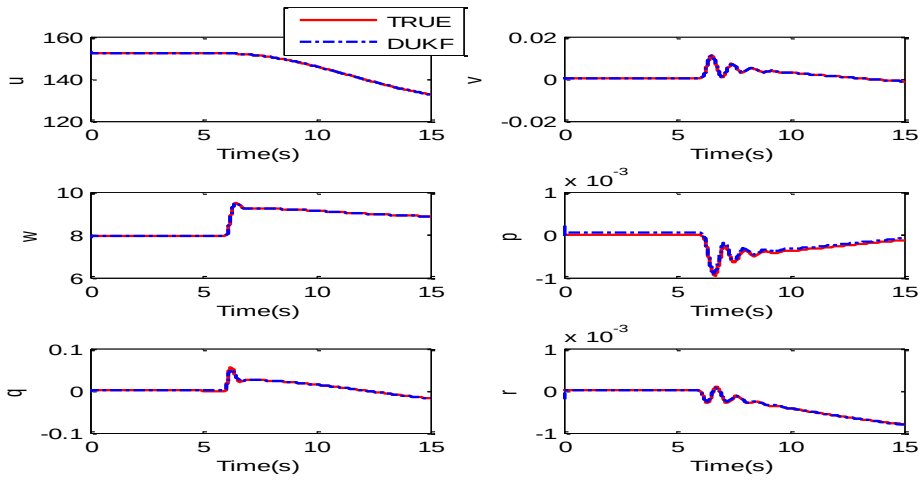

Figure 5-7 States estimation (u, w, v, p, q, r)

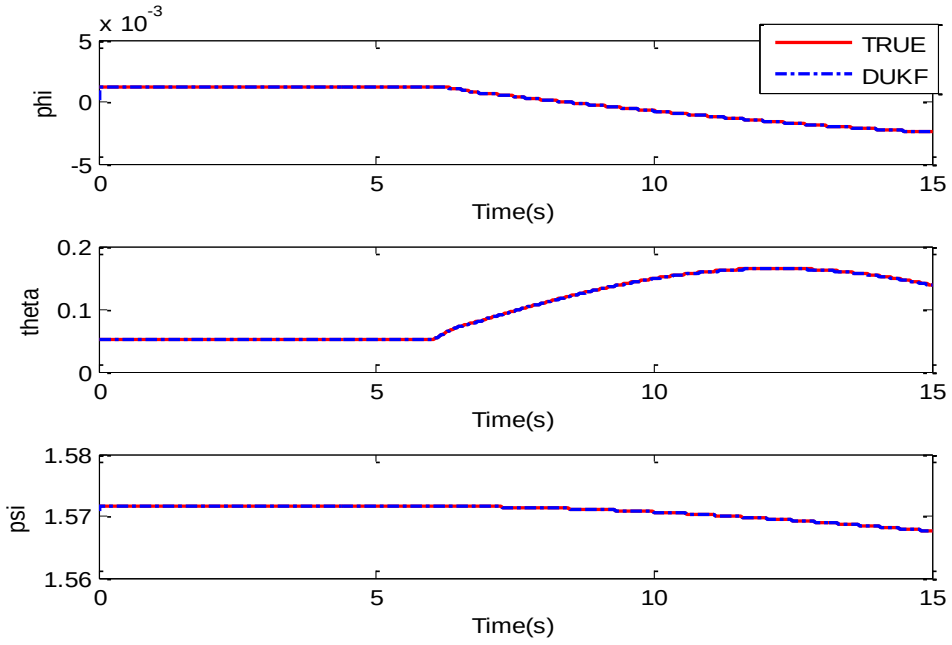

Figure 5-8 States estimation (ϕ, θ, ψ)

On Figure 5-7 and Figure 5-8, the red solid line represents the system outputs and the blue dash-dot line represents the state estimation results of DUKF. The measured and estimated states of DUKF are almost equal making it hard to see the difference between.

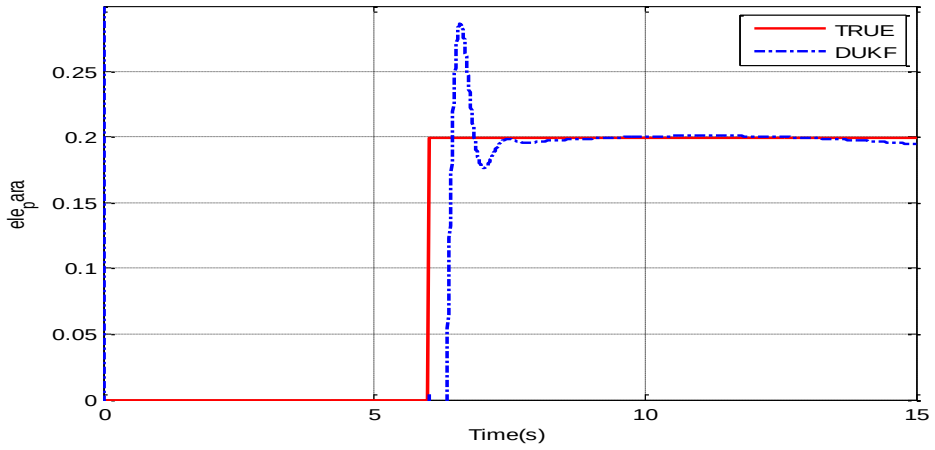

Figure 5-9 δ_e control effectiveness estimation (20% partial loss occurred at 6 seconds)

Figure 5-9 shows that DUKF can detect and diagnosis the partial loss occurred at 6 seconds, and the delay is less than one second.

From Figure 5-7 to Figure 5-9, it can be observed that the DUKF can correctly estimate all the states and fault parameters within the given time limits in the nonlinear model, and it is very easy to implement the DUKF in the nonlinear model since it does not need to linearize the nonlinear model. It can be seen that the DUKF is a powerful recursive parameter estimation algorithm that improves the reliability of parameter estimates in the nonlinear systems.

5.2.2 Application with a GTM LPV Model

In the LPV model, the experiment starts with the initial states $X = \begin{bmatrix} 0 & 0 & 0 & 0 \end{bmatrix}^T$. The measurement interval is $T = 0.01s$. The test scenario is that a 20% loss of control effectiveness fault in elevator occurred at 6 sec. The UKF parameters are listed as follows:

$$\begin{cases} \alpha = 1 \\ \beta = 2 \\ k = 3 - L, L = 12 \\ Rr_{ukfpe} = diag\left(\left(1/0.99983 - 1 \right) \right) Pw \\ \mathrm{Re}_{ukfpe} = 0.0091^2 I_{4\times 4} \\ Rv = 0.01^2 I_{4\times 4} \\ Rn = I_{4\times 4} \\ Px = I_{4\times 4} \\ Pw = 0.001 I_{2\times 2} \end{cases}$$

The ATSEKF and DUKF use the measured outputs and outputs of LPV, and the state estimation and parameter estimation of the ATSEKF and DUKF will be presented below.

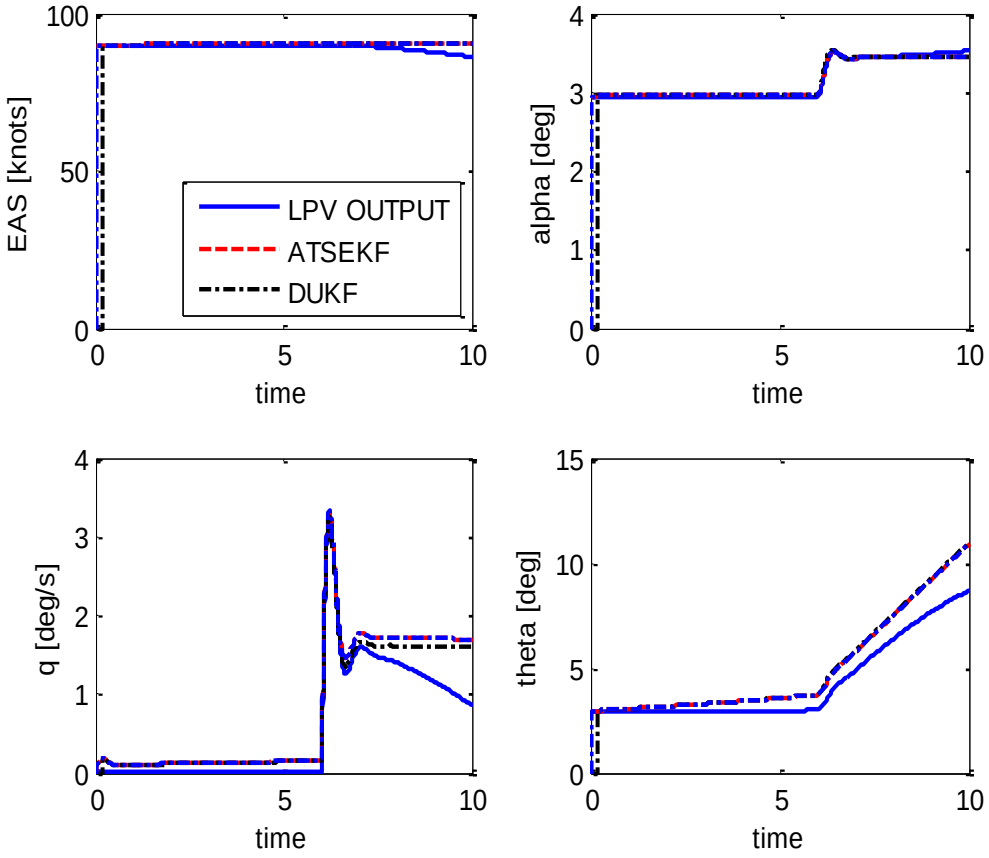

Figure 5-10 States estimation (EAS, α, q, θ)

On Figure 5-10, the estimation outputs of ATSEKF and DUKF are close to the LPV output at the beginning, but with the time growing, the ATSEKF and DUKF cannot follow the output of LPV model. On Figure 5-11 below, the blue solid line represents the true partial loss, the red dash line represents the parameter estimation of DUKF and the black dash-dot line represents the parameter estimation of ATSEKF. The estimation results demonstrate that DUKF and ATSEKF can detect and isolate the partial loss fault precisely when δ_e occurs partial loss of 20% at 6 seconds.

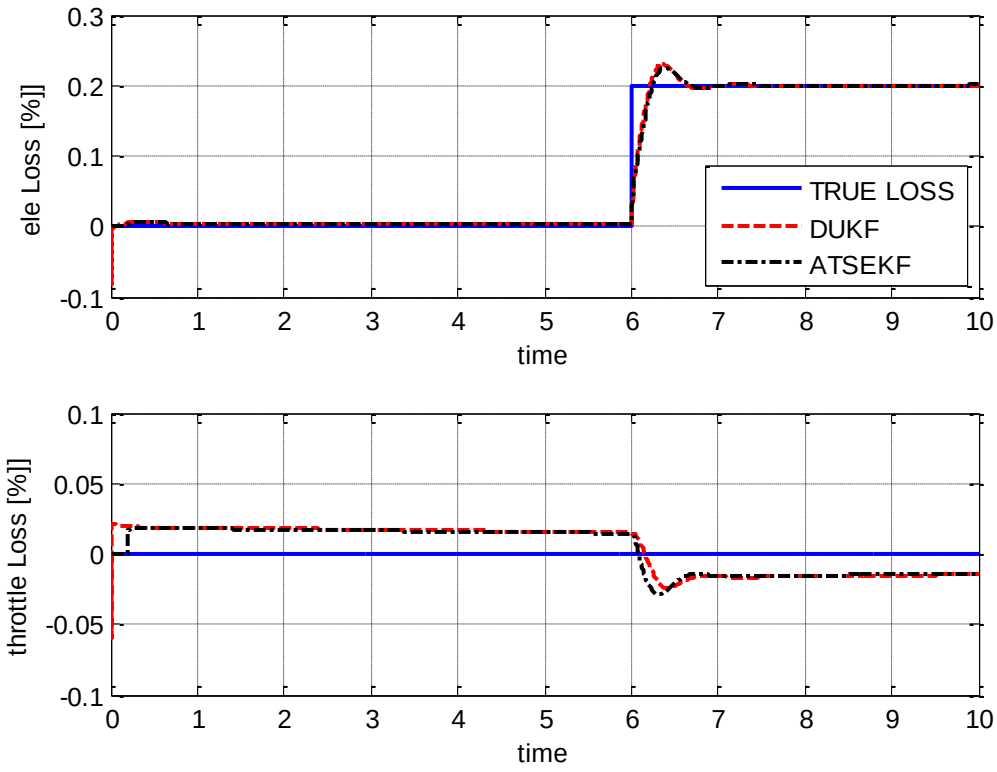

Figure 5-11 δ_t and δ_e control effectivness estimation (δ_e partial loss of 20% at 6 sec)

On Figure 5-10 to Figure 5-11 show that the states estimation of the ATSEKF and DUKF in the GTM LPV environment matched well with the measured outputs and also it filtered the measurement noises and two Kalman algorithms detect and identify the fault precisely when the elevator encounters a partial loss.

For the nonlinear model of GTM, the results showed that estimated effectiveness had a large jump when the fault occurred, but it became stable in a short time. The LPV model showed that DUKF and ATSEKF had similar parameter estimation accuracy, since the LPV model had simplified the nonlinear model greatly.

5.3 Application to Boeing 747 Model

The implementation of Kalman filter in Boeing 747 model is different from the implementation of quad-rotor UAV model. The measurement time interval is $T = 0.02s$. The simulation starts from the initial condition as $X = \begin{bmatrix} 0.0162 & 0 & 230 & 0.0162 & 7000 \end{bmatrix}^T$. The UKF parameters are chosen as:

$$\begin{cases} \alpha = 1 \\ \beta = 2 \\ K = 3 - L, L = 15 \\ Rr_{ukfpe} = diag\left(\left(1/0.99975 - 1 \right) \right) * Pw \\ \mathrm{Re}_{ukfpe} = 0.0091^2 I_{5\times5} \\ Rv = 0.01^2 I_{5\times5} \\ Rn = I_{5\times5} \\ Px = I_{5\times5} \\ Pw = 0.001 I_{3\times3} \end{cases}$$

The first test scenario is that δ_s control effectiveness encounters a partial loss of 50% at 15 seconds.

On Figure 5-12, the red solid line represents the true measured states, the blue dash-dot line represents the estimated states of DUKF and the black dash line is the estimated states of ATSEKF. The simulation results show that the measured and estimated states of ATSEKF and UDKF are almost equal making it hard to see the difference between them.

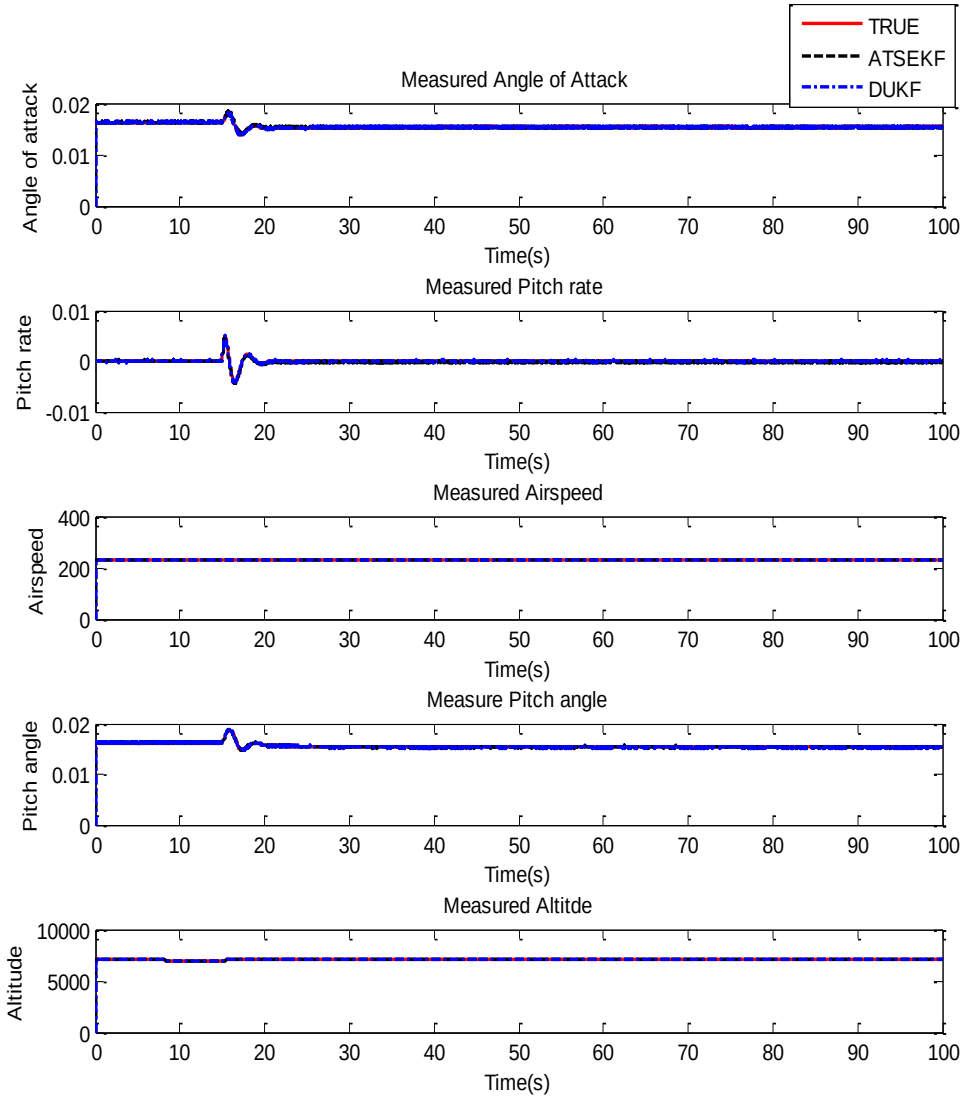

Figure 5-12 States estimation $(\alpha, V, q, \theta, h_e)$

In Figure 5-13, the black dash line is the parameter estimated by ATSEKF, the blue dash-dot line represents the parameter estimated by DUKF, and the red solid line shows the partial loss of the true fault parameter. The simulation results show that both algorithms can estimate the partial loss occurred on δ_s in the Boeing 747 nonlinear model correctly.

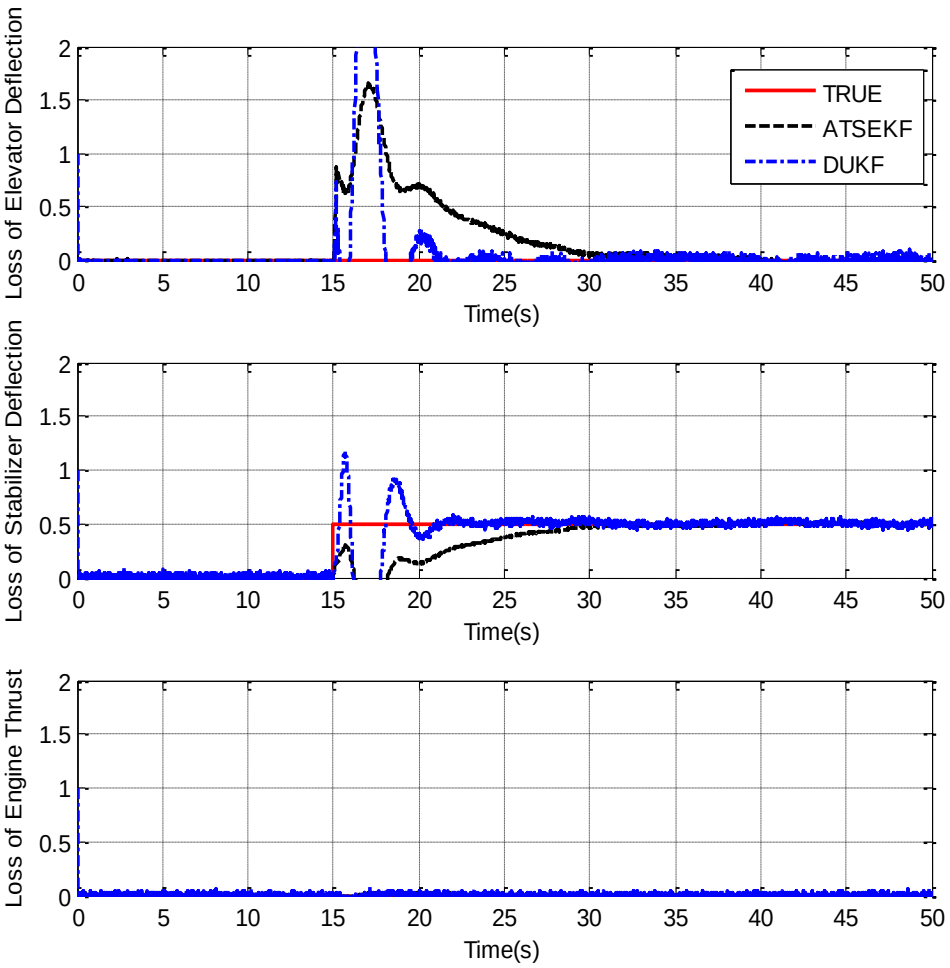

Figure 5-13 (δ_e, δ_s, T) control effectiveness estimation (δ_s encounters a partial loss of 50% at 15 seconds)

From Figure 5-12 to Figure 5-13, only one of (δ_e, δ_s, T) encounters a partial loss and others are working properly. From the above simulation results, it can be easily seen that the outputs of the ATSEKF and DUKF matched well with measured outputs and also it filtered the measurement noises. The DUKF converges faster than the ATSEKF in the parameter estimation.

The second test scenario is that δ_e encounters 40% partial loss at 20 seconds, δ_s encounters 50% partial loss at 20 seconds and T encounters 20% partial loss at 30 seconds.

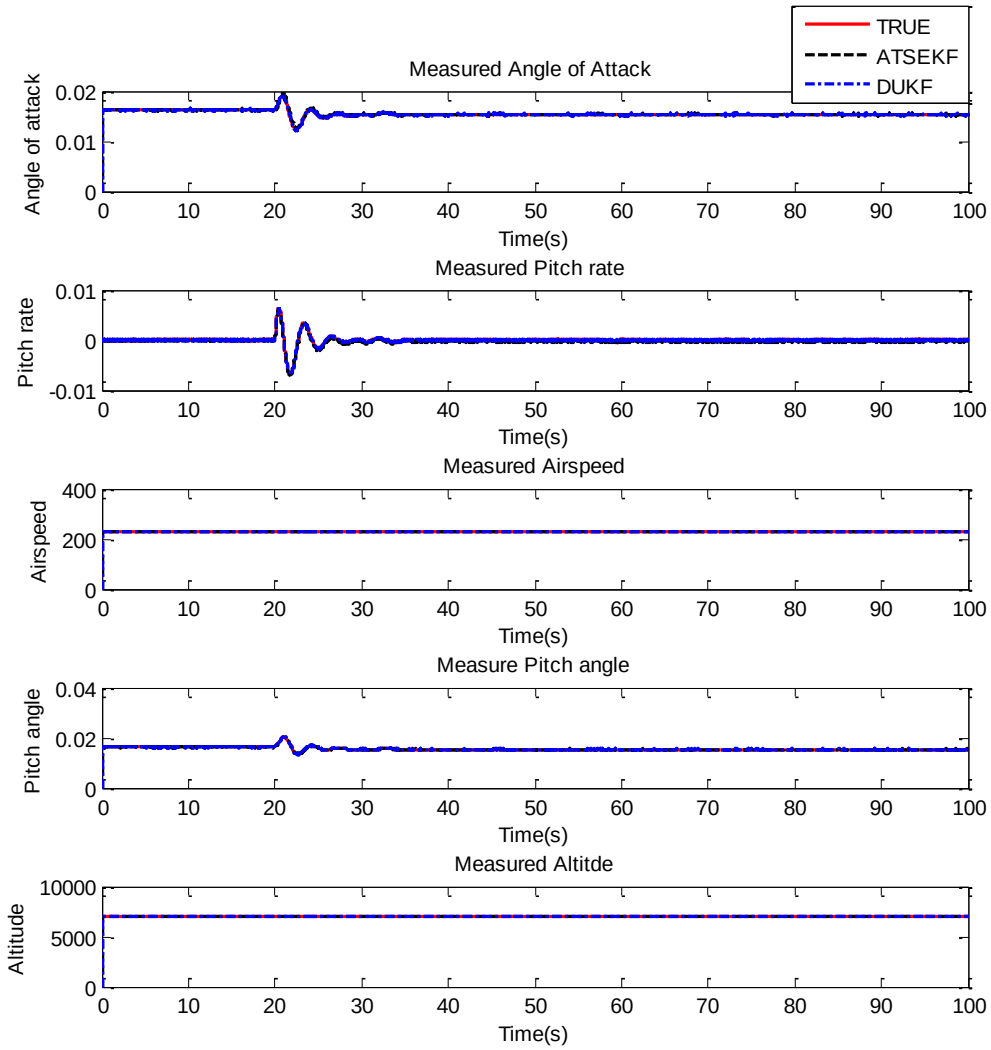

Figure 5-14 States estimation $(\alpha, V, q, \theta, h_e)$

On Figure 5-14, the measured and estimated states are almost equal making it hard to view the difference between them.

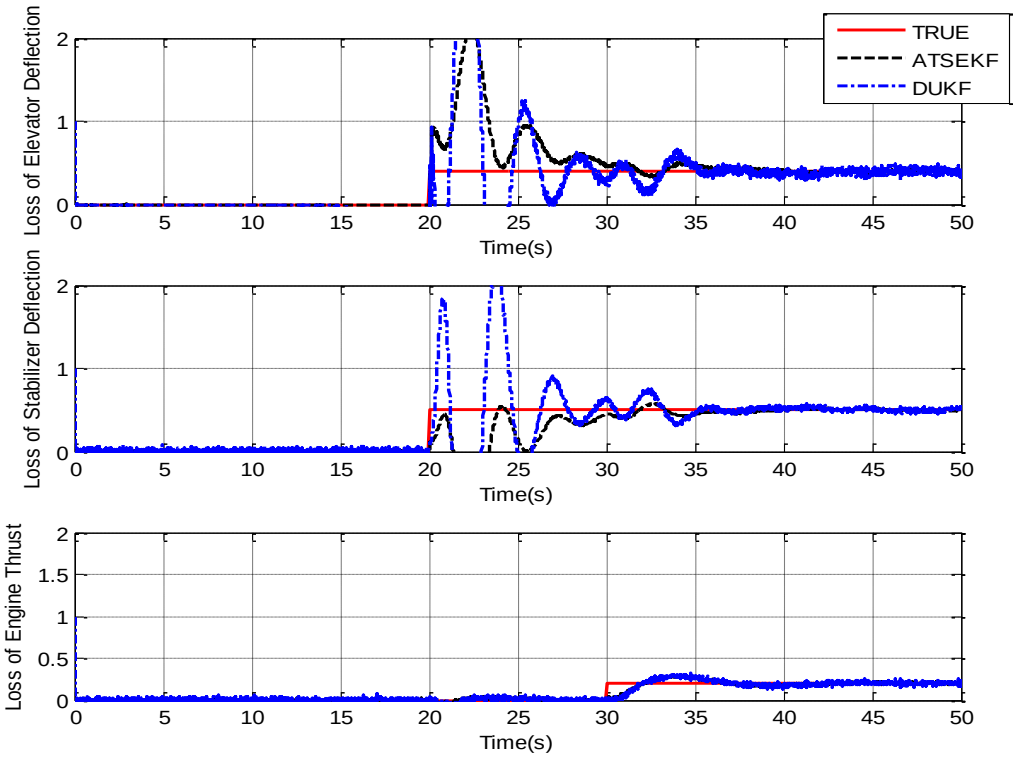

Figure 5-15 (δ_e, δ_s, T) control effectiveness estimation ((δ_e, δ_s, T) encounters a partial loss)

Figure 5-15 presents that both ATSEFK and DUKF can estimate all partial losses occurred in the Boeing 747 nonlinear model correctly.

From Figure 5-12 to Figure 5-15, it can be concluded that for the estimation of the Boeing 747 aircraft with nonlinear model, the simulation showed that the DUKF has better performance. DUKF can estimate the magnitude of fault very accurately in the nonlinear model. The results have shown that ATSEKF and DUKF can not only track the reference input effectively but also detect and diagnose the occurrence of the actuator faults in the quad-rotor UAV and Boeing 747 Simulink models.

5.4 Comparison of ATSEKF and DUKF

The simulation results show that DUKF is able to obtain better estimation accuracy of fault magnitudes compared with ATSEKF. For the linearized model of Boeing 747, both DUKF and ATSEKF can obtain accurate estimation of fault magnitudes, but in terms of time to convergence, DUKF is faster than ATSEKF.

DUKF is the fastest algorithm in terms of time of convergence. However, DUKF is computationally more expensive, especially for nonlinear models whose coefficients are implemented by lookup tables in the Matlab/Simulink. The reason is that DUKF algorithm requires the $2L+1$ sigma points, where N is the dimension of the augmented state. These $2L+1$ sigma points join the measurement update and time update, so it makes the computation $2L+1$ times larger than that of ATSEKF. Because ATSEKF linearizes the system at each sample point, it could lead to a poor performance by introducing unknown errors in the covariance of the transformed distribution. Furthermore, ATSEKF has to linearize the system at each time step, so it makes the implementation more difficult. After comparing the DUKF and ATSEKF, it is easy to find that the DUKF is better than ATSEKF, but with the cost of high demand for computation.

5.5 Summary

This chapter presents the simulation results of quad-rotor UAV, GTM UAV and Boeing 747. The estimations of GTM nonlinear model and LPV model produced similar results as Boeing 747. The simulation results indicated that ATSEKF and DUKF can correctly estimate all the states and fault parameters within the given time limits. However, the simulation results with quad-rotor UAV show that ATSEKF and DUKF

can detect the faults, but cannot identify the faults satisfactorily since quad-rotor UAV is a highly coupling nonlinear system.

6 Conclusions and Future Works

6.1 Conclusions

This thesis presented results from an on-line FDD design based on nonlinear recursive state and parameter estimation in the framework of discrete-time stochastic system. The estimation performance of two Kalman filters, namely ATSEKF and DUKF, were also compared.

Simulation evaluation results in Chapter 5 show that both ATSEKF and DUKF are very successful in terms of states estimation. However, there are some differences in parameters estimation performance. In terms of convergence, DUKF is faster than ATSEKF in parameter estimation. It should be pointed that the DUKF is a powerful recursive state and parameter estimation algorithm that improves the reliability of parameter estimates in the nonlinear systems. The DUKF has the advantage that it separates state estimation and parameter estimation which is more accurate compared with ATSEKF. The DUKF can use the nonlinear model of the system directly with no need to linearize the nonlinear system, so the DUKF is easier in algorithm implementation. The drawback of the DUKF is that it is more time-consuming, especially when the number of system states and the number of parameters to be estimated increase.

6.2 Future Works

In terms of faults, this work only considers partial loss type of faults. Other types of actuator faults need to be taken into consideration as one of the future works. Only actuator faults have been considered while the other faults are assumed to functional

normally. In reality, faults can occur also in the sensor and system components. Development of new FDD schemes for sensor and system component fault including wing/body damages will be another future works. Improvement of the robustness and performance of the ATSEKF and DUKF algorithms, development of computationally more efficient DUKF algorithm, as well as integration of the FDD schemes with fault tolerant control are also some future works.

References

[1] Y. M. Zhang and J. Jiang, "Design of Proportional-Integral Reconfigurable Control Systems via Eignestructure Assignment", *Proceedings of the 2000 American Control Conference*, Chicago, WN, June 2000, pp. 3732-3736.

[2] Y. M. Zhang and J. Jiang, "Design of Integrated Fault Detection, Diagnosis and Reconfigurable Control Systems", *Proceedings of the 38th IEEE Conference on Decision and Control*, Phoenix, AZ, December 1999, pp. 3587-3592.

[3] Y. M. Zhang and J. Jiang, "Bibliographical Review on Reconfigurable Fault-Tolerant Control Systems", *IFAC Annual Reviews in Control*, Vol. 32, Issue 2, December 2008, pp. 229-252.

[4] M. M. Mahmoud, J. Jiang and Y. M. Zhang, *Active Fault Tolerant Control Systems*, Springer-Verlag, Berlin, 2003.

[5] Y. M. Zhang and J. Jiang, "Active Fault-tolerant Control System against Partial Actuator Failures", *IEE Proceedings of Control Theory and Applications*, Vol. 149, Issue 1, January 2002, pp. 95-104.

[6] P. M. Frank, "Fault Diagnosis in Dynamic System using Analytical and Knowledge-based Redundancy – A Survey and Some New Results", *IFAC Automatica*, Vol. 26, Issue 3, 1990, pp. 459-474.

[7] C. Angeli, "On-Line Fault Detection Techniques for Technical Systems: A Survey", International Journal of Computer Science & Application, Vol. 1, Issue 1, 2004, pp. 12-30.

[8] V. J. Jategaonkar, *Flight Vehicles System Identification*, AIAA Inc., Reston, VA, August 2006, pp. 219-264.

[9] R. E. Kalman, "A New Approach to Linear Filtering and Prediction Problems", *Research Institute for Advanced Study, Transactions of the ASME-Journal of Basic Engineering*, March 1960, pp. 35-45.

[10] S. G. Mohinder and P. A. Angus, *Kalman Filtering Theory and Practice using MATLAB*, Wiley-IEEE Press, September 9, 2008.

[11] M. I. Ribeiro, "*Kalman and Extended Kalman Filters: Concept, Derivation and Properties*", PhD Dissertation, Institute for Systems and Robotics, Instituto Superior Tecnico, February 2004, Chapters 1 and 4.

[12] S. Haykin, *Kalman Filters*, in Kalman Filtering and Neural Networks, John Wiley & Sons, Inc. 2001, Chapter 1.

[13] www.AirDisaster.com (accessed on June 2010).

[14] J. H. Gove and D. Y. Hollinger, "Application of a Dual Unscented Kalman Filter for Simultaneous State and Parameter Estimation in Problem of Surface-Atmosphere Exchange", *Journal of Geophysical Research*, Vol. 111, D08S07. 2006.

[15] N. E. Wu and Y. M. Zhang, "Control Effectiveness Estimation using an Adaptive Kalman Estimator", *Proceedings of the 1998 IEEE ISIC/CIRA/ISAS Joint Conference*, Gaithersburg, MD, September 14-17, 1998.

[16] http://www.patentstorm.us/patents/4043526/description.html (accessed on June 2010).

[17] L. H. Chiang, E. L. Russell and R. D. Braatz, *Fault Detection and Diagnosis in Industrial Systems*, Springer, January 2001, pp. 3, pp. 174.

[18] Y. M. Zhang and N. E Wu, "Fault Diagnosis for a Ship Propulsion Benchmark: Part I", *Proceedings of the 14th Triennial World Congress*, Beijing, P. R. China, July 5-9, 1999, pp. 569-574.

[19] J. Y. Keller and M. Darouach , "Optimal Two-stage Kalman Filter in the Presence of Random Bias", *Automatica*, Vol. 33, Issue 9, pp. 1745-1748, 1997.

[20] C. V. Matthew, L. S. Jana and D. H. Christopher, "Unscented Kalman Filtering for Spacecraft Attitude State and Parameter Estimation", *Proceedings of the AAS/AISS Space Flight Mechanics Conference*, Maui, Hawaii, February 8-12, 2004.

[21] K. Xiong, C. W. Chan and H. Y. Zhang, "Unscented Kalman Filter for Fault Detection", *IFAC 16th World Congress*, Prague, 2005.

[22] J. Qi, Z. Jiang and X.G. Zhao, "Adaptive UKF and Its Application in Fault Tolerant Control of Rotorcraft UAV", *AIAA Guidance, Navigation and Control Conference and Exhibit*, Hilton Head, South Carolina, August 20-23 2007.

[23] E.A Wan and R. Merwe, *The Unscented Kalman Filter*, in Kalman Filtering and Neural Networks, John Wiley & Sons, Inc. 2001, Chapter 7.

[24] S. J. Julier and J. K. Uhlmann, "A new Extension of the Kalman Filter to Nonlinear Systems", *Proceedings of AeroSense: 11th Int. Symp. Aerospace/Defense Sensing*, Simulation and Controls, 1997, pp. 182-193.

[25] E. A. Wan and R. V. Merwe, "The Unscented Kalman Filter for Nonlinear Estimation", *Adaptive Systems, Signal Processing, Communications, and Control Symposium*, Lake Louise, AB, Canada, October 2000.

[26] E. A. Wan and A. T. Nelson, *Dual Extended Kalman Filter Methods*, in Kalman Filtering and Neural Networks, John Wiley & Sons, Inc. 2001.

[27] H. Bouadi, M. Bouchoucha, and M. Tadjine, "Sliding Mode Control based on Backstepping Approach for an UAV Type-Quadrotor", *International Journal of Applied Mathematics and Computer Sciences*, Vol. 4, Issue 1, 2007, pp. 12-17.

[28] T. Madani and A. Benallegue, "Control of a Quadrotor Mini-Helicopter via Full State Backstepping Technique", *Proceedings of the 45th IEEE Conference on Decision & Control*, Manchester Grand Hyatt Hotel, San Diego, CA, USA, December 13-15 2006, pp. 1515-1520.

[29] H. Voos, "Nonlinear State-Dependent Riccati Equation Control of a Quadrotor UAV", *Proceeding of the 2006 IEEE International Conference on Control Applications*, Munich, Germany, October 4-6, 2006, pp. 2547-2552.

[30] T. L. Jordan, J. V. Foster, R. M. Bailey, and C. M. Belcastro, "AirSTAR: A UAV Platform for Flight Dynamics and Control System Testing", *25th AIAA Aerodynamic Measurement Technology and Ground Testing Conference*, San Francisco, CA, 2006.

[31] J. Y. Shin, "*Worst-Case Analysis and Linear Parameter-Varying Gain-Scheduled Control of Aerospace Systems*", PhD Dissertation, University of Minnesoda, 2000, pp. 108-141.

[32] A. Marcos and G. J. Balas, "Development of Linear-Parameter-Varying Models for Aircraft", *Journal of Guidance, Control, and Dynamics*, Vol. 27, Issue 2, 2004, pp. 218-228.

[33] R. Pandita, A. Chakraborty, P. Seiler and G. J. Balas, "Reachability and Region of Attraction Analysis Applied to GTM Dynamic Flight Envelop Assessment", *AIAA Guidance, Navigation, and Control Conference*, Chicago, Illinois, August 2009, pp. 10-13.

[34] A. M. Esteban and G. J. Balas, "Linear Parameter Varying Modeling of the Boeing 747-100/200 Longitudinal Motion", *AIAA Guidance, Navigation, and Control Conference*, Montreal, Canada, August 2001, pp. 4317-4347.

[35] M. Ruschmann, J. Huang, and N. E. Wu, "Probing the NASA Generic Transport Aircraft in Real-Time for Health Monitoring", *Proceedings of the 48th IEEE Conference on Decision and Control*, December 2009, pp. 4920-4929.

[36] A. M. Esteban, "*A Linear Parameter Varying Model of the Boeing 747-100/200 Longitudinal Motion*", M.Sc. Thesis, University of Minnesota, 2001.

[37] G. Chowdhary and R. Jategaonkar, "Aerodynamic Parameter Estimation from Flight Data Applying Extended and Unscented Kalman Filter", *AIAA Atmospheric Flight Mechanics Conference and Exhibit*, August 2006.

[38] H. Alwi, "*Fault Tolerant Sliding Mode Control Schemes with Aerospace applications*", PhD Dissertation, Department of Engineering, University of Leicester, UK, February 2008.

[39] G. S. Becker, "*Quadratic Stability and Performance of Linear Parameter Dependent Systems*", PhD Dissertation, Department of Mechanical Engineering, University of California-Berkeley, USA, 1993.

[40] R. Isermann, "Model-based Fault Detection and Diagnosis - Status and Applications", *Annual reviews in Control*, Vol. 29, Issue 1, 2005, pp. 71-85 .

[41] V. Venkatasubramanian, R. Rengaswamy and S. N. Kavuri, "A Review of Process Fault Detection and Diagnosis Part II: Qualitative Models and Search Strategies", *International Journal of Computers and Chemical Engineering*, Vol. 27, Issue 3, March 2003, pp. 313-326.

[42] V. Venkatasybramanian, R. Rengaswamy, S. N. Kavuri and K. W. Yin, "A Review of Process Fault Detection and Diagnosis Part III: Process History Based Methods", *International Journal of Computers and Chemical Engineering*, Vol. 27, Issue 3, March 2003, pp. 327-346.

[43] R. J. Montoya, W. E. Howell, W. T. Bundick, A. J. Ostroff, R. M. Hueschen, and C. M. Belcastro, "Restructurable Controls", Tech. Rep. NASA CP-2277, *Proceedings of a workshop held at NASA Langley Research Center*, Hampton, Virginia, September 21-22, 1982.

[44] R. Isermann, "Supervision, Fault-detecion and Fault-diagnosis Methods – An Introduction", *Control Engineering Practice*, Vol. 5, Issue 5, May 1997, pp. 639-652.

[45] C. Angeli, "On-line Fault Detection Techniques for Technical Systems: A Survey", *International Journal of Computer Science & Applications*, Vol. 1, Issue 1, 2004, pp. 12-30.

[46] Y. M. Zhang, "Active Fault-tolerant Control Systems: Integration of Fault Diagnosis and Reconfigurable Control (Invited Plenary Lecture)", *The 8th Conference on Diagnostics of Processes and Systems*, Slubice, Poland, September 2007.

[47] Q. S. Yang, "Model-based and Data Driven Fault Diagnosis Methods with Applications to Process Monitoring", *PhD Dissertation*, Case Western Reserve University, May 2004.

[48] V. Venkatasubramanian, R. Rengaswamy, K.Yin etc, "A Review of Process Fault Detection and Diagnosis Part I: Quantitative Model-based Methods", *Computers in Chemical Engineering*, Vol. 27, Issue 3, March 2003, pp. 293-311.

[49] M. Iri, K. Aoki, E. O'Shima, "An Algorithm for Diagnosis of System Failures in the Chemical Process," *Computers and Chemical Engineering*, Vol. 3, Issue 1, 1979, pp. 489-493.

[50] B. E. Kelly and F. P. Lees, "The Propagation of Faults in Process Plants: 2.Fault Tree Synthesis," *Reliability Engeering*. Vol. 16, Issue 1, 1986, pp. 39-62.

[51] J. D. Kleer and S. Brown, "A Qualitative Physics Based on Confluences," *Artificial Intelligence*, Vol. 24, 1984, pp.7-83.

[52] F. R. Hampel, E. M. Ronchetti, P. J. Rousseeuw, and W. Stahel, *Robust Statistics: The Approach Based on Influence Functions*, Wiley, New York, 1986.

[53] B. Kuipers, "Qualitative Simulation," *Artificial Intelligence*, Vol. 29, 1986, pp. 289-338.

[54] O. Raiman, "Order of Magnitude Reasoning," *Proceedings of the National Conference on Artificial Intelligence*, AAAI, August 1986, pp. 100-104.

[55] N. E. Wu, Y. M. Zhang and K. Zhou, "Detection, Estimation, and Accommodataion of Loss of Control Effectiveness," *International Journal of Adaptive Control and Signal Processing*, Vol 14, Issue 7, 2000, pp. 775-795.

[56] J. Y. Keller and M. Darouach, "Optimal Two-stage Kalman Filter in Presence of Random Bias," *Automatica*, Vol. 33, Issue, 1997, pp. 1745-1748.

[57] G. Becker, "*Quadratic Stability and Performance of Linear Parameter Dependent Systems*," PhD Dissertation, Department of Engineering, University of California, Berkeley, 1993.

[58] Y. M. Zhang, X. R. Li, X. D. Yang and H. C. Zhang, "Detection and Identification of Bias Faults in Nonlinear Systems," *Proceedings of the 35th IEEE Conf. on Decision and Control*, Kobe, Japan, December. 11-13, 1996, pp. 638-639

[59] B. Friedland, "Treatment of Bias in Recursive Filter," *IEEE Trans. on Automatic Control,* , Vol 14, Issue 4, August 1969, pp. 359-367.

[60] www.people.com.cn/GB/junshi/1079/2998865.html (accessed on November 2010)

[61] www.nasa.gov/centers/langley/news/factsheets/AvSP-factsheet.html (accessed on November 2010)

[62] R. Isermann and P. Balle, "Trends in the Application of Model-based Fault Detection and Diagnosis of Technical Processes," *Control Engineering Practice*, Vol 5, 1997, pp. 709-719.

[63] C. Edwards, T. Lombaerts and H. Smaili, *Fault Tolerant Flight Control: A Benchmark Challenge*, Springer-Verlag, 2010, pp. 54.

[64] http://en.wikipedia.org/wiki/American_Airlines_Flight_191 (accessed on January 2011)

Publications during the thesis work

- L. Ma and Y. M. Zhang, "Fault Detection and Diagnosis for GTM UAV with Dual Unscented Kalman Filter", Presented at the *2010 AIAA Guidance, Navigation, and Control Conference*, Toronto, Ontario, Canada, 2-5 Aug. 2010, AIAA-2010-7884.
- L. Ma and Y. M. Zhang, "DUKF-based Fault Detection and Diagnosis for GTM UAV using Nonlinear and LPV Models", Presented at the Diagnosis and Monitoring in Mechatronic Systems Symposium in *2010 IEEE/ASME International Conference on Mechatronic and Embedded Systems and Applications*, 15-17 July 2010, Qingdao, P. R. China.